

Speeding Up a Single Ion Thermal Machine

BACHELOR THESIS

for obtaining the degree Bachelor of Science

Institute of Physics

University of Kassel

Topic: Transient Non-Confining Potentials for Speeding
Up a Single Ion Heat Pump

Submitted from: Moritz Göb
Address: Angersbachstraße 2
34127 Kassel

Matriculation Number: 33385187
Email Address: moritzgoeb@physik.uni-kassel.de

Department: Institut für Physik
Experimentalphysik I

Examiner: Prof. Dr. Kilian T. T. Singer
Prof. Dr. Martin E. Garcia

Supervisor: Prof. Dr. Kilian T. T. Singer

Submitted: 21.10.2019

Declaration

Herewith I declare, that I have produced the presented paper myself and solely with the aid of the means permitted by the examination regulations of the University of Kassel. The literature used is indicated in the bibliography. I have indicated literally or correspondingly assumed contents as such.

LOCATION, DATE

Moritz Göb

Abstract

The working cycle of the single-atom heat engine [Roß16b] proves the functionality of a Stirling engine on a single-atom level. To investigate quantum thermodynamics at this level, Carnot or Otto engine are of interest. These engines are composed of adiabatic expansion/compression. An adiabatic change of a physical system usually has a long evolution time. By exploiting invariants a significant speedup can be obtained, without losing efficiency due to friction. Here the general method for obtaining such shortcuts is discussed on the basis of a single ion trapped in a tapered Paul trap. By allowing non-confining potentials for short times, an even higher speedup is obtained.

Zusammenfassung

Der Arbeitszyklus der Ein-Atom-Wärmekraftmaschine [Roß16b] beweist die Funktionalität einer Wärmekraftmaschine mit nur einem Atom. Dennoch wird diese nur als Stirling-Maschine betrieben. Um die Quantenthermodynamik auf dieser Ebene zu untersuchen, müssen Carnot- oder Ottowärmekraftmaschinen implementiert werden. Diese Maschinen benutzen adiabatischer Expansion und Kompression. Eine adiabatische Veränderung eines physikalischen Systems dauert normalerweise eine verhältnismäßig lange Zeit. Durch die Ausnutzung von Invarianten kann eine signifikante Beschleunigung dieser Prozesse erzielt werden, ohne die Effizienz aufgrund von Verlusten zu verringern. In dieser Arbeit wird das allgemeine Verfahren zum Bestimmen solcher Protokolle auf der Basis eines einzelnen Ions diskutiert, das in einer konischen Paul-Falle gefangen ist. Indem für kurze Zeit nicht fangende Potenziale zugelassen werden, wird eine noch höhere Beschleunigung erhalten.

Contents

Declaration	III
1. Introduction	1
1.1. Motivation	1
1.2. Trapped ions	1
1.2.1. Paul traps	2
1.2.2. Calcium ion	4
1.3. Heat engines	5
1.3.1. The Carnot cycle	5
1.3.2. The Otto cycle	7
1.3.3. The Stirling cycle	8
1.3.4. Single-atom heat engine	9
2. Quantum dynamics	11
2.1. Heisenberg equation of motion	11
2.1.1. Ehrenfest theorem	12
2.2. Density operators and Liouville equation	13
3. Shortcut to adiabaticity	15
3.1. Adiabaticity	15
3.2. Lewis-Riesenfeld invariants	16
3.3. Invariant-based reverse Engineering	16
3.4. Reverse engineering of Gaussian states	18
3.4.1. Coherent states	18
3.4.2. Thermal states	18
3.4.3. Quantum dynamical evolution of Gaussian states	19
4. Numerical methods	21
4.1. Strömer-Verlet method	21
4.2. Gradient ascent/descent method	22
4.2.1. Reduction of radio frequency power and limited radio frequency amplitudes	24
4.2.2. Robustness	24
5. Results	25
5.1. Proposed experimental implementation	25
5.2. Robustness improvements	26
5.3. STA in comparison	27
5.3.1. Fidelity evaluation	29
5.4. Confirmation of trapping condition	31

6. Outlook	33
6.1. Single-atom heat engine as sensible quantum heat probe	33
A. Appendix	35
A.1. Implementation of the Strömer-Verlet method	35
B. List of publications	37
Bibliography	38

1. Introduction

1.1. Motivation

The investigation of quantum thermodynamics on the single-particle level requires sophisticated systems. Usually, thermodynamics are best investigated in heat engines. To go to the quantum limit, one needs to perform experiments on single particles. A promising platform is trapped ions because it is well established and therefore has many tools available. A recent breakthrough demonstrated that a heat engine can be implemented in a single ion [Roß16b]. The single-atom heat engine, which is described in Section 1.3.4, was operated in the classical regime as a Stirling engine. Hence the Carnot engine has a fundamental relation to the second law of thermodynamics, it is especially interesting to be implemented in an experiment. Such an engine is composed of adiabatic processes, which usually require a long evolution time. This yields a longer interaction time which gives rise to more perturbations from the environment.

To minimize such perturbations and therefore minimize friction, it is desirable to perform these processes as fast as possible. A significant speedup can be obtained by exploiting shortcuts to adiabaticity (STA) [Che10; Tor12; Tor13a; Pal16; Tor18]. Such protocols can be exploited not only to guarantee a fast friction-less transition, but also yield a much shorter cycle time. This will boost the power of the single-atom heat engine. Furthermore, if the cycle is reversed a speedup for a single ion heat pump can be obtained.

This thesis is structured in the following way. In this chapter, the underlying concepts of Paul traps, as well as trapped ions themselves, will be explained in Section 1.2. Furthermore, in Section 1.3 the working principle of heat engines will be illustrated. In 2 general concepts of quantum dynamics are summarized. The method to construct a shortcut to adiabaticity is demonstrated in Chapter 3. In order to obtain a good understanding of the dynamic of the system during the shortcut protocol and optimize it, numerical investigations are needed. These are described in Chapter 4. In Chapter 5 the results of the investigation are presented. An outlook is given Chapter 6.

1.2. Trapped ions

Trapped ions are a suitable platform for many applications. Ground state preparation can be performed [Lei03] and can be coupled to engineered reservoirs [Tur00]. Also, they are well suited for quantum information processing. High fidelity one- and two-qubit gates have been realized [Møl99; Sch03; Lem13]. Recently it was shown,

that a chain of four ions can be prepared in a maximally entangled state [Kau17]. Furthermore, a clock with a systematic uncertainty below 10^{-18} was implemented with trapped $^{27}\text{Al}^+$ [Bre19].

1.2.1. Paul traps

A Paul trap can confine a single particle in three dimensions by only using electric potentials. It is also possible to confine particles inside a Penning trap, by applying magnetic static potentials [Bro86]. Hence *Earnshaw's theorem* prohibits confinement of an electric charge in all three dimensions by applying a static electric potential, one needs to exploit fast oscillating radio frequency (rf) potentials. One can make a generalized ansatz [Sin10].

$$\begin{aligned} \Phi(x, y, z, t) = & \frac{U_{\text{dc}}}{2} (\alpha_{\text{dc}}x^2 + \beta_{\text{dc}}y^2 + \gamma_{\text{dc}}z^2) \\ & + \frac{U_{\text{rf}}}{2} \cos(\omega_{\text{rf}}t) (\alpha_{\text{rf}}x^2 + \beta_{\text{rf}}y^2 + \gamma_{\text{rf}}z^2) \end{aligned} \quad (1.1)$$

U_{dc} describes a constant direct current trapping voltage and U_{rf} is the rf trapping voltage, which oscillates with a frequency ω_{rf} . The potential needs to fulfill the Laplace equation in a charge-free space.

$$\Delta\Phi(x, y, z, t) = 0 = U_{\text{dc}} (\alpha_{\text{dc}} + \beta_{\text{dc}} + \gamma_{\text{dc}}) + U_{\text{rf}} \cos(\omega_{\text{rf}}t) (\alpha_{\text{rf}} + \beta_{\text{rf}} + \gamma_{\text{rf}}) \quad (1.2)$$

One can separate the coefficient in a time-dependent and in a time-independent part.

$$\begin{aligned} 0 &= \alpha_{\text{dc}} + \beta_{\text{dc}} + \gamma_{\text{dc}} \\ 0 &= \alpha_{\text{rf}} + \beta_{\text{rf}} + \gamma_{\text{rf}} \end{aligned} \quad (1.3)$$

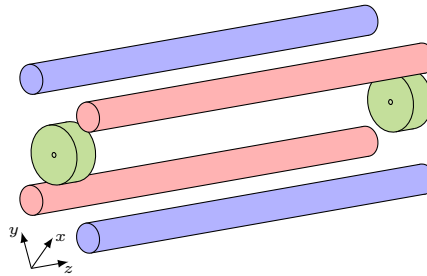


Figure 1.1.: Schematic of a linear Paul trap.

Many configurations are possible. As an example, a linear Paul trap will be discussed, which is depicted in Figure 1.1. We choose $\gamma_{\text{rf}} = 0$. Therefore, the remaining parameters need to fulfill the constraints imposed by the Laplace equation (1.3). The remaining parameters satisfy

$$\begin{aligned} -\alpha_{\text{dc}} &= \beta_{\text{dc}} + \gamma_{\text{dc}} \\ \alpha_{\text{rf}} &= -\beta_{\text{rf}} \end{aligned} \quad (1.4)$$

This yields dynamical confinement in the x - y plane and static confinement along the z -axis. A classical equation of motion for a particle with mass m and charge q can be derived.

$$m \frac{\partial^2 \vec{r}}{\partial t^2} = q \nabla \Phi(\vec{r}, t), \quad (1.5)$$

with $\vec{r} = (x, y, z)^T$. This yields a set of uncoupled Mathieu differential equations. The solutions can be found in the literature [Lei03; Sin10].

$$\frac{d^2 r_i}{d\xi^2} + [a_i - 2q_i \cos(2\xi)] r_i(\xi) = 0, \quad (1.6)$$

with $i = x, y$ and $2\xi = \omega_{\text{rf}} t$. The parameter a_i and q_i are determined by the geometry of the trap. In the case of this example, they can be derived to be

$$\begin{aligned} q_x &= \frac{2|q|U_{\text{rf}}\alpha_{\text{rf}}}{m\omega_{\text{rf}}^2}, & a_i &= -\frac{4|q|U_{\text{dc}}\alpha_{\text{dc}}}{m\omega_{\text{rf}}^2} \\ q_y &= -\frac{2|q|U_{\text{rf}}\beta_{\text{rf}}}{m\omega_{\text{rf}}^2}, & a_i &= \frac{4|q|U_{\text{dc}}\beta_{\text{dc}}}{m\omega_{\text{rf}}^2}. \end{aligned} \quad (1.7)$$

Stable solutions can be found for $0 \leq \beta_i \leq 1$, with $\beta_i = \sqrt{a_i + \frac{q_i^2}{2}}$. When $|a_i|, q_i^2 \ll 1$ a solution of Equation (1.6) can be found.

$$r_i(t) = r_i(0) \cos(\omega_i t) \left(1 + \frac{q_i}{2} \cos(\omega_{\text{rf}} t) \right) \quad (1.8)$$

The ion trajectory is composed of a secular harmonic oscillation at the frequency $\omega_i = \beta_i \frac{\omega_{\text{rf}}}{2}$ and micromotion which are fast but small oscillations at the frequency of the radio drive. The confinement along the z axis is a harmonic potential with the frequency

$$\omega_z = \sqrt{\frac{|q|U_{\text{dc}}\gamma_{\text{dc}}}{m}}. \quad (1.9)$$

The motion in radial in radial direction can be assumed to be harmonic, hence the micromotion are comparably small. Furthermore, the micromotion is comparatively fast and vanishes when taking the time average over one period of $\omega_{x,y}$. This yields a pseudo potential in the radial direction.

$$\Phi_{\text{p}}(x, y) = \frac{|q| |\nabla \Phi(x, y, z, 0)|^2}{4m\omega_{\text{rf}}^2} \quad (1.10)$$

It has been experimentally demonstrated, that the micromotions can be minimized to a great extent by using additional electrodes [Ber98]. It can therefore be well approximated by a harmonic potential.

Funnel-shaped Paul trap

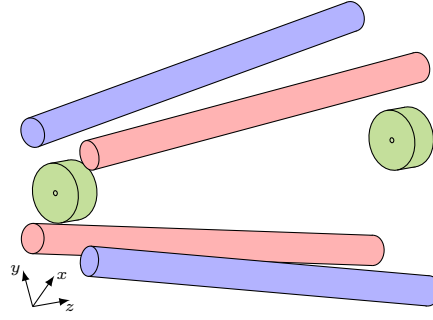


Figure 1.2.: Schematic of a linear Paul trap.

The funnel-shaped Paul trap is very similar to a linear Paul trap, which is described above. The electrodes are placed in an angle ϑ with respect to the z axis of the trap. This yields a tapered RF potential.

$$\Phi(x, y, z, t) \propto \frac{U_{\text{rf}} \cos(\omega_{\text{rf}} t)}{(r_0 + z \tan(\vartheta))^2} (x^2 - y^2) + \frac{U_{\text{dc}}}{z_0^2} z^2 \quad (1.11)$$

Here r_0 describes the distances of the RF electrodes and z_0 the distance of the DC electrodes. A pseudo potential can be derived for this set up as well using Equation (1.10).

$$\Phi_{\text{p}} = \frac{m}{2} \frac{\omega_{x,0}^2 x^2 + \omega_{y,0}^2 y^2}{(r_0 + z \tan(\vartheta))^4} + \frac{m}{2} \omega_z^2 z^2 \quad (1.12)$$

Here $\omega_{i,0}$ denotes the trapping frequency in radial direction at $z = 0$. One thing of note, that the radial trapping frequency is dependent on the axial position. The tapering of the trap leads to an effective coupling of the radial and the axial degrees of freedom [Roß16a].

1.2.2. Calcium ion

For the reduction of complexity in experiments, earth-alkali ions are used, because of their hydrogen-like structure. Furthermore ions without nuclei spin are favorable hence the hyper-fine structure is non-existing. The electron configuration of a $^{40}\text{Ca}^+$ is $[\text{Ar}]4s^2S_{1/2}$. In Figure 1.3 the energy levels are depicted

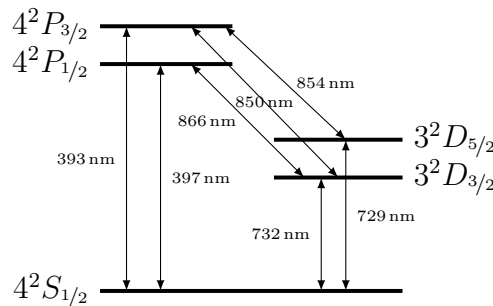


Figure 1.3.: Energy level scheme of $^{40}\text{Ca}^+$.

Not all of the transitions in Figure 1.3 are relevant. In fact it is sufficient to use four of the depicted transitions to obtain full control of the system. The transition $4s^2S_{1/2} \leftrightarrow 4p^2P_{1/2}$ has a short lifetime of $\tau_P = 6.9\text{ ns}$ [Het15]. This short lifetime can be utilized for laser cooling [Lei03]. The ion decays from the $4p^2P_{1/2}$ to the $3d^2D_{3/2}$ state with a probability of 6.4% [Ram13]. Hence further relaxation to the ground state is dipole forbidden, this state has long life time of $\tau_D = 1.18\text{ s}$ [Kre05]. In order to counteract this decoherence, a light field near 866 nm is used to re-pump the decayed population to the $4p^2P_{1/2}$ state.

1.3. Heat engines

Heat engines are one of the crucial driving forces behind social development. The development of steam power engines was crucial for further technical developments, which sparked the industrial revolution. Before this, heat engines were only of interest to researchers. But due to the more efficient design, the steam power engines could generate enough work to provide factories with it. The quest for higher and higher powers was sparked. Further breakthroughs were the development of the combustion engine by Nicolaus August Otto in 1876 [Sas62] and the self-combustion engine by Rudolf Diesel in 1893 [Die93]. This enabled the development of cars and trucks, which made transport of people and goods much easier.

A heat engine consists in general of a working agent, which is connected to a flywheel, and a cold and hot reservoir. The reservoirs provide the heat engine with energy, which drives the working agent. The flywheel allows one to extract work from the heat engine.

To validate theoretical research in the field of quantum thermodynamics, which has been going on for quite some time, smaller and smaller engines are needed. Therefore, miniaturization is needed to be able to operate a heat engine in the quantum realm. A recent breakthrough made a proof of principle of a single-atom heat engine [Roß16b; Roß16a]. This heat engine still works in the regime of classical thermodynamics, but has all the necessary tools to reach the quantum limit.

The Carnot and Otto cycle will be discussed in Section 1.3.1 in a classical sense. Furthermore, the working principle of the single-atom heat engine will be described in Section 1.3.4.

1.3.1. The Carnot cycle

The Carnot cycle is a heat engine cycle, which was formulated by Sadi Carnot [Car72] and is still the subject of much recent research [Cur75; Gev92a; Ben00; Esp10a; Esp10b; Ma17; Ma18; Dan19a]. However, it needs to be perfectly reversible, which is not feasible for experimental implementation. Because even the slightest friction leads to irreversible entropy production. Furthermore, finite-time effects also need to be considered, hence perfect thermalization is only reached at infinite time [Gev92a; Gev92b].

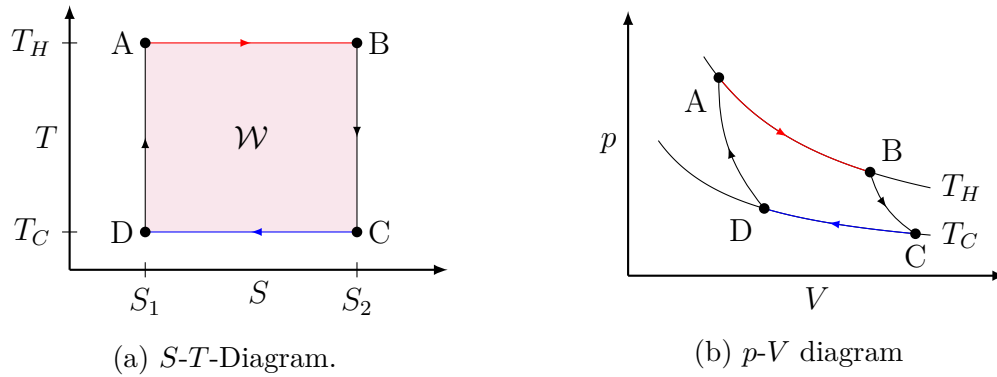


Figure 1.4.: Depiction of the Carnot cycle in a (a) T - S diagram and in a (b) p - V diagram.

The Carnot cycle, which is depicted in Figure 1.4, is composed of four processes. These are described below.

$A \rightarrow B$	isothermal expansion	The working agent is in contact with the hot reservoir at temperature T_H and work is transferred reversibly from the hot reservoir to it.
$B \rightarrow C$	adiabatic expansion	The working agent is decoupled from bath and adiabatically expanded until it reaches the temperature of the cold reservoir T_C .
$C \rightarrow D$	isothermal compression	The working agent is in contact with the cold bath at temperature T_C , to which work is transferred from the working agent.
$D \rightarrow A$	adiabatic compression	The working agent is decoupled from the cold reservoir and adiabatically compressed until it reaches the temperature of the hot reservoir T_H .

To quantify the quality of a heat engine the efficiency η is used. It is defined as the ratio of the work \mathcal{W} performed by the working agent and the heat flowing in the system \mathcal{Q}_{AB} . The heat flowing into the system can be computed by

$$\mathcal{Q}_{AB} = T_H \cdot \Delta S, \quad (1.13)$$

with $\Delta S = (S_2 - S_1)$, hence the system is decoupled from the environment during the adiabatic expansion. The work transferred from the hot to the cold reservoir can be expressed as

$$\mathcal{W} = (T_H - T_C) \cdot \Delta S. \quad (1.14)$$

From this expressions, the efficiency of the Carnot cycle can be η_C can be computed.

$$\eta_C = \frac{(T_H - T_C)}{T_C} = 1 - \frac{T_H}{T_C} \quad (1.15)$$

It can be concluded from the second law of thermodynamics, that the Carnot efficiency yields a tight classical bound for any heat engine. That is due to the use of solely reversible adiabatic and isothermal processes.

$$\boxed{\eta \leq 1 - \frac{T_H}{T_C}} \quad (1.16)$$

Perfect reversible thermalization can only be reached after infinite time. Therefore, the output power, which is defined by the work per cycle \mathcal{W} divided by the time per cycle τ_{cyc} , from a perfect reversible heat engine approximates zero, hence $\tau_{\text{cyc}} \rightarrow \infty$ [Cal85]. In order to best utilize the output of the heat engine, one wants to operate it at maximal efficiency at maximum power. Because such an engine runs at finite times, the isothermal processes will not be reversible. Such an engine is called a *endoreversible engine*. The Curzon-Ahlborn limit yields a classical tight bound for such the efficiency at maximal power [Cur75; Nov58].

$$\eta_{\text{CA}} = 1 - \sqrt{\frac{T_H}{T_C}} \quad (1.17)$$

It is important to note, that the Carnot efficiency, as well as the Curzon-Ahlborn limit, is solely dependent on the temperatures of the cold and hot reservoirs.

1.3.2. The Otto cycle

The Otto cycle is one of the most used in modern technology. It approximates the cycle of a gasoline combustion engine, which is installed in cars. As well as the Carnot cycle, the Otto cycle is investigated in recent research [Den13; Roß14; Kos17; Aba19; Çak19]. A schematic depiction of the Otto cycle is found in Figure 1.5.

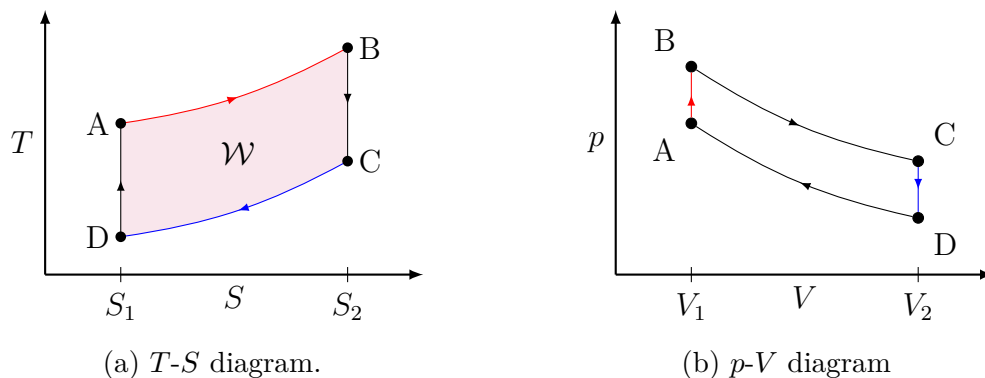


Figure 1.5.: Depiction of the Otto cycle in a (a) T - S diagram and in a (b) p - V diagram.

The Otto cycle is composed of four strokes which are described below. The heat transfer between the working agent and the reservoirs does not occur at a constant temperature. Therefore, one needs to account for this change at every infinitesimal step by integrating over the changing temperature. The efficiency of

A → B	isochoric heating	Heat is transferred from the hot reservoir to the working agent while the volume is kept constant.
B → C	adiabatic expansion	The working agent is adiabatic expanded till V_2 is reached.
C → D	isochoric cooling	Heat is transferred from the working agent to the cold reservoir while the volume is kept constant.
D → A	adiabatic compression	The working agent is adiabatic compressed till V_1 is reached.

an Otto cycle is solely dependent on the property of the working agent. For an ideal gas, the Otto efficiency can be derived to be

$$\epsilon_{\text{Otto}} = 1 - \left(\frac{V_2}{V_1} \right)^{\frac{c_p - c_v}{c_v}}, \quad (1.18)$$

where c_p denotes the isobaric and c_v the isochoric heat capacity [Cal85].

Quantum harmonic Otto cycle

The quantum harmonic Otto cycle is the quantum version of the previously described Otto cycle. A straight forward approach is seeking analogues for each process. Hence the system is viewed as a harmonic oscillator, and exterior parameters as e.g. volume are not clearly defined [Kos17]. Instead frequency and occupation number are used to describe the cycle. The "cold" frequency ω_c corresponds to V_1 and the "hot" frequency ω_h to V_2 . The heat transfer is expressed as the difference of the occupation number $\Delta n = n_h - n_c$, with $n_i = 1/(\exp[\hbar\omega_i/k_bT_i] - 1)$. The work per cycle is obtained.

$$\mathcal{W}_{\text{cyc}} = \hbar\Delta\omega\Delta n, \quad (1.19)$$

with $\Delta\omega = \omega_h - \omega_c$ [Kos17]. The efficiency of the quantum harmonic oscillator becomes

$$\eta_{\text{Otto}} = 1 - \frac{\omega_c}{\omega_h} \leq \eta_{\text{CA}}. \quad (1.20)$$

1.3.3. The Stirling cycle

The Stirling cycle is not that prominent in modern technology and is usually known from entry-level experimental physics lecture. But still has many interesting applications. For example, a Stirling engine, which is heated by solar power, can be utilized to propel a generator [Kon03]. Furthermore, since a Stirling engine doesn't use combustion, it makes lower noise and can be used environments with fire hazards or where oxygen is a crucial resource. Such an environment is found in submarines.

Therefore a Stirling engine is well suited to propel a submarine [Nil88]. The Stirling cycle is still subject to recent research [Wu98; Yin17; Yin18].

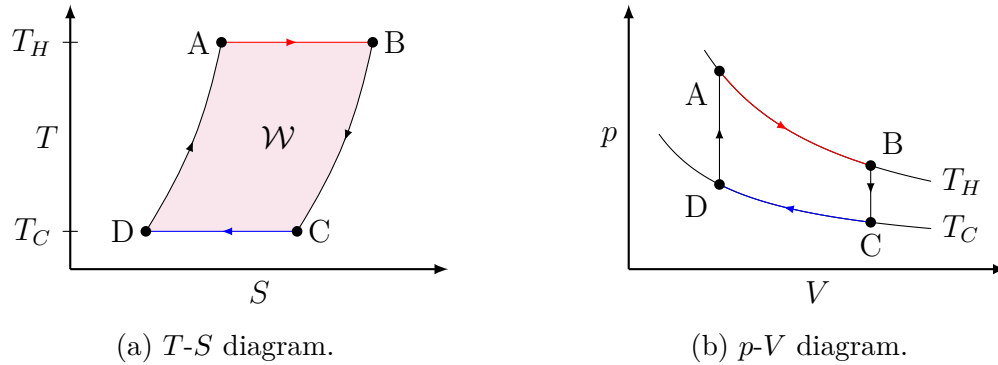


Figure 1.6.: Depiction of the Stirling cycle in a (a) T - S diagram and in a (b) p - V diagram.

The Stirling cycle, which is depicted in Figure 1.6, is composed of four processes, which are described below.

$A \rightarrow B$	isothermal expansion	The working agent is in contact with the hot reservoir at temperature T_H and work is transferred reversibly from the hot reservoir to it.
$B \rightarrow C$	isochoric expansion	The working agent is decoupled from bath and adiabatically expanded until it reaches the temperature of the cold reservoir T_C .
$C \rightarrow D$	isothermal compression	The working agent is in contact with the cold bath at temperature T_C , to which work is transferred from the working agent.
$D \rightarrow A$	isochoric compression	The working agent is decoupled from the cold reservoir and adiabatically compressed until it reaches the temperature of the hot reservoir T_H .

Hence the Stirling cycle includes isothermal expansion and compression like a Carnot cycle, the same notion as discussed in Section 1.3.1 applies here.

1.3.4. Single-atom heat engine

To test thermodynamics in the quantum regime, heat engines need to be realized in quantum systems. In 2016 a major breakthrough was achieved. A heat engine was implemented with a single $^{40}\text{Ca}^+$ ion as the working agent. The ion was trapped in a funnel-shaped ion trap, which is described in Section 1.2.1, to couple the axial degree of freedom to the radial. [Roß16a]

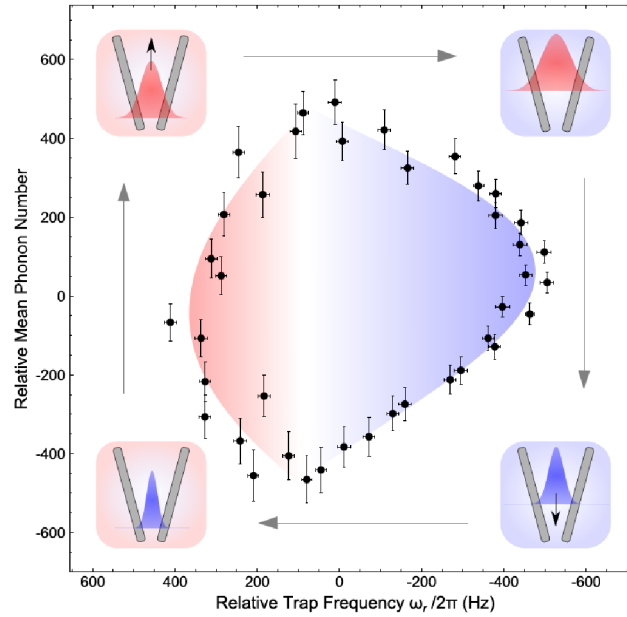


Figure 1.7.: Working cycle of the single-atom heat engine [Roß16b].

The working cycle of the single-atom heat engine is depicted in Figure 1.7. Because the motional state of the ion can be described as a harmonic oscillator, a representation in frequency and mean phonon number was chosen by the authors. A sterling cycle is realized by switching between hot and cold reservoir. The hot reservoir is implemented as noise on the trapping electrodes, which heat the radial degrees of freedom of the ion. The Doppler cooling laser is interacting constantly interacting with the ion. Thus the cold bath is implemented by switching off the noise on the trapping electrodes.

The ion, which has a temperature of n_H , moves away from the apex, hence the displacement force is increased due to a broader wave packet in radial direction. This yields a lowering of the the radial frequency, until ω_c is reached. The ion is then Doppler cooled, till it reaches n_C . The force on the ion reduces. Due to the lowered force, the ion moves towards the apex of the taper until the frequency ω_c is reached. By applying noise to the electrodes the ion is heated till it reaches n_H and the cycle starts over again.

The single-atom heat engine performed at an efficiency of $\eta_{\text{SIHE}} = 2.8\%$ with a power of $P = 3.42 \cdot 10^{-22}$ J [Roß16b].

2. Quantum dynamics

2.1. Heisenberg equation of motion

To understand and describe the time-dependency of quantum-mechanical system, a description is needed. The temporal evolution of a state $|\psi\rangle \in \mathcal{H}$ can be described by the time-dependent Schrödinger equation [Sak17, p. 66-73].

$$i\hbar \frac{d}{dt} |\psi(t)\rangle = \hat{H}(t) |\psi(t)\rangle. \quad (2.1)$$

Assuming, that the Hamiltonian \hat{H} is time-independent, Equation (2.1) simplifies to the time-independent Schrödinger equation.

$$i\hbar \frac{d}{dt} |\psi(t)\rangle = \hat{H} |\psi(t)\rangle. \quad (2.2)$$

This equation can be solved by defining an unitary time-evolution operator $\hat{U}(t, t_0 = 0) = e^{-\frac{i}{\hbar} \hat{H}t}$. The time-evolution of a state is then given by

$$|\psi(t)\rangle = \hat{U}(t, 0) |\psi(0)\rangle \quad (2.3)$$

Each measurement result of a quantum system is described as an expectation value of an hermitian operator. The expectation value of a time-independent hermitian operator $\hat{A}^{(S)} \in L(\mathcal{H})$ can be expressed as

$$\begin{aligned} \langle \psi(t) | \hat{A}^{(S)} | \psi(t) \rangle &= \langle \hat{U}(t, 0) \psi(0) | \hat{A}^{(S)} | \hat{U}(t, 0) \psi(0) \rangle \\ &= \langle \psi(0) | \hat{U}^\dagger(t, 0) \hat{A}^{(S)} \hat{U}(t, 0) | \psi(0) \rangle \\ &= \langle \psi(0) | \hat{A}^{(H)}(t) | \psi(0) \rangle = \langle \hat{A}^{(H)}(t) \rangle_{|\psi(0)\rangle}. \end{aligned} \quad (2.4)$$

The superscript S and H denotes, that the operator is written in the Schrödinger or Heisenberg picture respectively. Hence these expectation values need to be equal and we can write the operator in the Heisenberg picture as

$$\hat{A}^{(H)}(t) = \hat{U}^\dagger(t, 0) \hat{A}^{(S)} \hat{U}(t, 0). \quad (2.5)$$

Taking the derivative with respect to time yields the following expression:

$$\frac{d\hat{A}^{(H)}(t)}{dt} = \frac{i}{\hbar} \hat{H} \hat{U}^\dagger(t) \hat{A}^{(S)} \hat{U}(t) + \hat{U}^\dagger(t) \frac{\partial \hat{A}^{(S)}}{\partial t} \hat{U}(t) - \frac{i}{\hbar} \hat{U}^\dagger(t) \hat{A}^{(S)} \hat{H} \hat{U}(t). \quad (2.6)$$

Hence $[\hat{U}(t), \hat{H}] = 0$ [Sak17, p. 83], Equation (2.6) can be rewritten to obtain the following expression.

$$\begin{aligned}
\frac{d\hat{A}^{(H)}(t)}{dt} &= \frac{i}{\hbar} \hat{H} \hat{U}^\dagger(t) \hat{A}^{(S)} \hat{U}(t) + \hat{U}^\dagger(t) \frac{\partial \hat{A}^{(S)}}{\partial t} \hat{U}(t) - \frac{i}{\hbar} \hat{U}^\dagger(t) \hat{A}^{(S)} \hat{U}(t) \hat{H} \\
&= \frac{i}{\hbar} \hat{U}^\dagger(t) \hat{H} \hat{A}^{(S)} \hat{U}(t) + \hat{U}^\dagger(t) \frac{\partial \hat{A}^{(S)}}{\partial t} \hat{U}(t) - \frac{i}{\hbar} \hat{U}^\dagger(t) \hat{A}^{(S)} \hat{H} \hat{U}(t) \\
&= \frac{i}{\hbar} \hat{U}^\dagger(t) \hat{H} \underbrace{\hat{U}(t) \hat{U}^\dagger(t)}_{=\hat{1}} \hat{A}^{(S)} \hat{U}(t) + \hat{U}^\dagger(t) \frac{\partial \hat{A}^{(S)}}{\partial t} \hat{U}(t) \\
&\quad - \frac{i}{\hbar} \hat{U}^\dagger(t) \hat{A}^{(S)} \hat{U}(t) \hat{U}^\dagger(t) \hat{H} \hat{U}(t) \\
&= \frac{i}{\hbar} \left(\hat{H}^{(H)}(t) \hat{A}^{(H)}(t) - \hat{A}^{(H)}(t) \hat{H}^{(H)}(t) \right) + \hat{U}^\dagger(t) \frac{\partial \hat{A}^{(S)}}{\partial t} \hat{U}(t) \\
&= \frac{i}{\hbar} \left[\hat{H}^{(H)}(t), \hat{A}^{(H)}(t) \right] + \hat{U}^\dagger(t) \frac{\partial \hat{A}^{(S)}}{\partial t} \hat{U}(t)
\end{aligned} \tag{2.7}$$

Here, $\hat{H}^{(H)}(t)$ denotes the representation of the Hamiltonian in the Heisenberg picture. Furthermore, the second term in the last row vanishes, if the operator \hat{A} is not explicitly time-dependent in the Schrödinger picture.

$$\boxed{\frac{d\hat{A}(t)}{dt} = \frac{i}{\hbar} \left[\hat{H}(t), \hat{A}(t) \right] + \frac{\partial \hat{A}(t)}{\partial t}}. \tag{2.8}$$

2.1.1. Ehrenfest theorem

By taking the expectation value of Equation (2.8), an expression for the time dependent expectation value is found. The states are taken in the Heisenberg picture and are therefore time-independent.

$$\left\langle \psi(0) \left| \frac{d\hat{A}(t)}{dt} \right| \psi(0) \right\rangle = \left\langle \psi(0) \left| \frac{i}{\hbar} \left[\hat{H}(t), \hat{A}(t) \right] \right| \psi(0) \right\rangle + \left\langle \psi(0) \left| \frac{\partial \hat{A}(t)}{\partial t} \right| \psi(0) \right\rangle \tag{2.9}$$

Hence state vectors are independent, the order of derivative and the expectation value can be exchanged.

$$\boxed{\frac{d}{dt} \langle \hat{A}(t) \rangle = \frac{i}{\hbar} \langle \left[\hat{H}(t), \hat{A}(t) \right] \rangle + \frac{\partial}{\partial t} \langle \hat{A}(t) \rangle} \tag{2.10}$$

It is particularly interesting to take a look at the time dependence of the momentum operator \hat{p} and position operator \hat{x} . The measurement of \hat{x} and \hat{p} can be easily implemented for most systems. For example the position of a trapped ion can be measured with a CCD camera [Glo15]. Furthermore, the momentum of the ion can be obtained by measuring the velocity dependent Doppler shift of a narrow transition, for example in an calcium ion the $4^2P_{1/2} \leftrightarrow ^2P_{1/2}$ or the $4p^2P_{1/2} \leftrightarrow 3d^2D_{3/2}$ transition [Roß15].

For a general Hamiltonian of the form $\hat{H} = \frac{\hat{p}^2}{2m} + V(\hat{x})$, the following expression is obtained for the time derivative of momentum and position operator.

$$\frac{d}{dt} \langle \hat{x} \rangle = \frac{1}{m} \langle \hat{p} \rangle \quad (2.11)$$

$$\frac{d}{dt} \langle \hat{p} \rangle = - \left\langle \frac{\partial V(x)}{\partial x} \right\rangle \quad (2.12)$$

To obtain an uncoupled differential equation, the derivative of Equation (2.11) is taken and Equation (2.12) is inserted.

$$\frac{d^2}{dt^2} \langle \hat{x} \rangle = - \frac{1}{m} \left\langle \frac{\partial V(x)}{\partial x} \right\rangle \quad (2.13)$$

This yields the classical equation of motion if $\left\langle \frac{\partial V(x)}{\partial x} \right\rangle = \frac{\partial}{\partial x} \langle V(x) \rangle$.

2.2. Density operators and Liouville equation

States in the Hilbert space give only a limited description of the full statistical behavior of quantum systems since they are only capable of modeling pure states. To depict mixed states as well, density operators need to be used. Mixed states can be interpreted as statistical admixture of quantum mechanical states. In a finite-dimensional Hilbert space the density operator is often referred to as the density matrix [Rei15]. For an arbitrary basis $\{|\psi_\ell\rangle\}$ of \mathcal{H} the density matrix can be written as

$$\hat{\rho} = \sum_{\ell} p_{\ell} |\psi_{\ell}\rangle \langle \psi_{\ell}|. \quad (2.14)$$

Here p_{ℓ} denotes the probability of finding the system in the pure state $|\psi_{\ell}\rangle$. Hence this is a probability distribution, $\forall \ell : p_{\ell} \geq 0$ and $\sum_{\ell} p_{\ell} = 1$ must hold. Furthermore, $\hat{\rho}$ is hermitian and positive-semi definite.

The expectation value of an operator $\hat{A} \in L(\mathcal{H})$ can be computed from the Hilbert-Schmidt norm $\langle \hat{A}, \hat{\rho} \rangle_{\text{HS}}$.

$$\langle \hat{A} \rangle = \langle \hat{A}, \hat{\rho} \rangle_{\text{HS}} = \text{tr} [\hat{A} \hat{\rho}]. \quad (2.15)$$

The dynamic of a density matrix is described by the Liouville-von Neumann equation. It can be derived by utilizing the time-dependent Schrödinger equation, after applying the product rule.

$$\boxed{\frac{\partial \hat{\rho}}{\partial t} = -\frac{i}{\hbar} [\hat{H}, \hat{\rho}]} \quad (2.16)$$

Equation (2.16) describes the evolution of a quantum system without dissipation. Compared to the Heisenberg equation of motion (Equation (2.8)), the Liouville-von Neumann equation has a strong resemblance. They only differ in sign. The reason for this is, that $\hat{\rho}$ has only a time-evolution according to the Schrödinger equation of motion and is not a dynamical observable in the Heisenberg picture, hence $\hat{\rho}$ is constructed from states in the Schrödinger picture [Sak17, p. 185].

3. Shortcut to adiabaticity

In this chapter, the formalism for constructing shortcuts to adiabaticity, as described in [Tor12; Tor13b; Cam14], is explained. In Section 3.1 a definition for adiabaticity is given. In Section 3.2 Lewis-Reisenfeld invariants are discussed and in Section 3.3, an invariant is found using the reverse engineering approach.

A major part of this chapter has been published in:

Transient Non-Confining Potentials for Speeding Up a Single Ion Heat Pump,
E. Torrontegui, S. T. Dawkins, M. Göb, K. Singer, *New Journal of Physics* **20**,
105001 (2018).

3.1. Adiabaticity

Adiabatic systems are closed systems, with no heat exchange with the environment. In thermodynamics, adiabatic processes are defined as processes, where there is no heat exchange [Bae09].

$$\dot{Q} = 0 \quad (3.1)$$

In quantum mechanics the adiabatic approximation is a common method to separate the dynamics of different processes, which evolves on different time scales. A "slow" change is on the scale of $T \gg 2\pi\hbar/\Delta E$, where ΔE is the difference in energy eigenvalues [Sak17, p. 346].

In the quantum harmonic Otto cycle [Kos17], the adiabatic assumption leads to a limitation of the cycle time $\tau_{\text{cyc}} \gg 4\pi/\Delta\omega$. The non-adiabatic parameter μ needs to fulfill

$$\mu = \frac{\dot{\omega}(t)}{\omega(t)^2} = \text{const.} \ll 1 \quad (3.2)$$

to be in the adiabatic limit. In this limit, no friction is generated and is therefore completely reversible.

As discussed in Section 1.3.1 this limits the output power P . To obtain higher power at the same amount of work \mathcal{W} one needs to minimize the cycle time [Den13; Bea16; Aba19]. On a shorter timescale the adiabatic condition is not satisfied and the dynamics are not separable anymore. To have an adiabatic process beyond the adiabatic limit a sophisticated protocol $\omega(t)$ needs to be found. Such a protocol is called a shortcut to adiabaticity (STA) [Che10; Tor12; Tor13b; Pal16; Tor18].

3.2. Lewis-Riesenfeld invariants

The Lewis-Riesenfeld theory is used to obtain a dynamical invariant $\hat{I}(t)$ of a quantum system, which evolves with a time-dependent Hamiltonian $\hat{H}(t)$. Such an invariant needs to be a unitary operator, which fulfills

$$\frac{d\hat{I}(t)}{dt} = \frac{\partial\hat{I}(t)}{\partial t} + \frac{i}{\hbar} [\hat{H}(t), \hat{I}(t)] = 0. \quad (3.3)$$

The dynamical invariant has the form

$$\hat{I}(t) = \sum_i \lambda_i |\phi_i\rangle\langle\phi_i|, \quad (3.4)$$

where $\{|\phi_i\rangle\}$ are the eigenvectors of $\hat{I}(t)$ with constant eigenvalues λ_n [Lew69]. Any solution of the time-dependent Schrödinger equation (Equation (2.1)) can be expanded in the eigenbases of the invariant.

$$|\Psi(t)\rangle = \sum_{\ell} c_{\ell} |\psi_{\ell}\rangle \quad \text{with} \quad |\psi_{\ell}\rangle = e^{i\alpha_{\ell}(t)} |\phi_{\ell}\rangle \quad (3.5)$$

The coefficients c_{ℓ} are constant and time independent. $\alpha_{\ell}(t)$ denotes the Lewis-Riesenfeld phase [Lew69].

$$\alpha_{\ell}(t) = \frac{1}{\hbar} \int_0^t \left\langle \phi_{\ell}(\tau) \left| i\hbar \frac{\partial}{\partial \tau} - \hat{H}(\tau) \right| \phi_{\ell}(\tau) \right\rangle d\tau \quad (3.6)$$

The representation of the density matrix in the eigenbases of the dynamic invariant $\langle\phi_j(t)|\hat{\rho}(t)|\phi_k(t)\rangle$ is computed by

$$\begin{aligned} \dot{\rho}_{jk}(t) &= i \left[\left\langle \phi_j(t) \left| i\hbar \frac{\partial}{\partial t} - \hat{H}(t) \right| \phi_j(t) \right\rangle - \left\langle \phi_k(t) \left| i\hbar \frac{\partial}{\partial t} - \hat{H}(t) \right| \phi_k(t) \right\rangle \right] \rho_{jk}(t) \\ \dot{\rho}_{jj}(t) &= 0. \end{aligned} \quad (3.7)$$

It becomes apparent, that the diagonal elements remain unchanged [Lew69]. This yields, that the populations, which are initialized in the eigenbasis of the invariant, stay in the instantaneous eigenstate without any transition. The off-diagonal elements depend on the time derivative of the Lewis-Riesenfeld phases [Lev18].

3.3. Invariant-based reverse Engineering

As discussed in the previous section, the populations of the instantaneous eigenstates do not change. To change the system without unwanted excitation, the commutator of the Hamiltonian and the invariant must vanish at starting time t_0 and final time t_f . This yields the so-called friction-less condition

$$\left[\hat{H}(t_0), \hat{I}(t_0) \right] = \left[\hat{H}(t_f), \hat{I}(t_f) \right] = 0. \quad (3.8)$$

This ensures that the system starts and ends in the eigenstates of the Hamiltonian. The construction of the invariant $\hat{I}(t)$ is demonstrated for an effective one-dimensional time-dependent harmonic oscillator.

$$\hat{H} = \frac{\hat{p}^2}{2m} + \frac{m}{2}\omega^2(t)\hat{q}^2. \quad (3.9)$$

To ensure a friction-less transition between $\hat{H}(t_0)$ and $\hat{H}(t_f)$ a proper invariant needs to be chosen. Such an invariant reads [Lew69]

$$\hat{I}(t) = \frac{1}{2m} \left[b(t)\hat{p} - m\dot{b}(t)\hat{q} \right]^2 + \frac{m}{2}\omega_0^2 \frac{\hat{q}^2}{b^2(t)}. \quad (3.10)$$

Function $b(t)$ needs to fulfill the Ermakov equation [Erm08]:

$$\ddot{b}(t) + \omega^2(t)b(t) = \frac{\omega_0^2}{b^3(t)}, \quad (3.11)$$

where ω_0 denotes the initial frequencies of the harmonic oscillator at t_0 . The boundary conditions, obtained from Equation (3.8), yields constraints for $b(t)$ at t_0 and t_f . For the sake of simplicity, $t_0 = 0$ is chosen, to obtain

$$\begin{aligned} b(0) &= 1, & \dot{b}(0) &= 0, & \ddot{b}(0) &= 0 \\ b(t_f) &= \gamma, & \dot{b}(t_f) &= 0, & \ddot{b}(t_f) &= 0, \end{aligned} \quad (3.12)$$

with the expansion/compression ratio $\gamma := \sqrt{\omega_0/\omega_f}$. The Lewis-Riesenfeld phase is computed using Equation (3.6).

$$\alpha_n(t) = -\omega_0 \left(n + \frac{1}{2} \right) \int_0^t d\tau \frac{1}{b^2(\tau)} \quad (3.13)$$

The wave function of an arbitrary state at a time can be obtained using Equation (3.5). The eigenfunction in spatial representation $\psi_n(q, t)$ is computed from $\langle \hat{q} | \psi_n(t) \rangle$.

$$\psi_n(q, t) = \left(\frac{m\omega_0}{\pi\hbar} \right)^{\frac{1}{4}} \frac{e^{i\left(\frac{m}{2\hbar}\right)\left(\frac{\dot{b}(t)}{b(t)} + i\frac{\omega_0}{b^2(t)}\right)q^2}}{\sqrt{2^n n! b(t)}} e^{-i\omega_0(n+\frac{1}{2})\int_0^t d\tau \frac{1}{b^2(\tau)}} H_n \left[\sqrt{\frac{m\omega_0}{\hbar}} \frac{q}{b(t)} \right], \quad (3.14)$$

where H_n denotes the Hermite polynomial of the n -th order. The average energy is computed from the expectation value of the Hamiltonian [Che10].

$$\langle \hat{H}(t) \rangle_n = \frac{(2n+1)\hbar}{4\omega_0} \left(\dot{b}^2(t) + \omega^2(t)b^2(t) + \frac{\omega_0^2}{b^2(t)} \right) \quad (3.15)$$

Furthermore, $\langle \hat{q} \rangle_n = 0$ and has a standard deviation of

$$\sigma_{\hat{q}} = \langle \hat{q}^2 \rangle = \int_{-\infty}^{\infty} dq q^2 |\psi_n(q, t)|^2 = \frac{\hbar b^2(t)}{m\omega_0} \left(n + \frac{1}{2} \right). \quad (3.16)$$

From Equation (3.16) a physical meaning for $b(t)$ can be deduced. $b(t)$ modulates the confinement and therefore changes the variance of a wave packet. Every function fulfilling the boundary conditions (Equation (3.12)) is a suitable drive

$$\omega^2(t) = \frac{\omega_0^2}{b^4(t)} - \frac{\ddot{b}(t)}{b(t)} \quad (3.17)$$

for the shortcut protocol, independent of the duration t_f . To obtain a solution for $b(t)$ a polynomial ansatz is made with $b(t) = \sum_{i=0}^5 a_i t^i$. To obtain a good solution there should be at least as many a_i as conditions on $b(t)$. The obtained system of linear equations is solved for the coefficients. The solution reads

$$b(t) = 6(\gamma - 1)\tau^5 - 15(\gamma - 1)\tau^4 + 10(\gamma - 1)\tau^3 + 1, \quad (3.18)$$

with $\tau = \frac{t}{t_f}$ [Tor18]. Hence $b(t)$ is not unique during the shortcut a more sophisticated function can be found, which also includes additional experimental constraints and allow for more optimization [Lev17; Lev18; Ste10; Che11; Tor17].

3.4. Reverse engineering of Gaussian states

3.4.1. Coherent states

The protocol, presented in Equation (3.17), is also suitable to apply not only on Fock states $|n\rangle$, but also oncoherent states [Pal16]. Hence $[\hat{H}(0), \hat{I}(0)] = 0$, the eigenbasis of the invariant and the Hamiltonian is common.

$$|\alpha(t)\rangle = e^{-\frac{|\alpha|^2}{2}} \sum_{n=0}^{\infty} \frac{\alpha^n}{\sqrt{n!}} |n(t)\rangle \quad (3.19)$$

After the shortcut is performed, the initial state $|\alpha(0)\rangle$ will evolve to

$$|\psi(t_f)\rangle = e^{-i\frac{g\omega_0}{2}} e^{-\frac{|\tilde{\alpha}|^2}{2}} \sum_{n=0}^{\infty} \frac{\tilde{\alpha}^n}{\sqrt{n!}} |\phi_n(t_f)\rangle = |\tilde{\alpha}(t_f)\rangle. \quad (3.20)$$

Where $g = \int_0^{t_f} d\tau \frac{1}{b^2(\tau)}$ and $\tilde{\alpha} = \alpha e^{-ig\omega_0}$. Due to the friction-less condition at t_f , the basis of \hat{I} and \hat{H} are the same. Thus a coherent state is obtained with frequency ω_f .

3.4.2. Thermal states

Thermal states are constructed as a function of the inverse temperature $\beta = \frac{1}{k_B T}$, where k_B is the Boltzmann constant. A thermal states can be written as [Nie09, p. 328]

$$\hat{\rho}_{\text{th}}(t) = \frac{e^{-\beta \hat{H}(t)}}{\text{tr} \left[e^{-\beta \hat{H}(t)} \right]}, \quad (3.21)$$

where the time-dependent Hamiltonian $\hat{H}(t)$ can be generally expressed in the Fock basis

$$\hat{H}(t) = \hbar\omega(t) \left(\hat{n}(t) + \frac{1}{2} \right). \quad (3.22)$$

The number operator \hat{n} has the eigenvectors $\hat{n} |n\rangle = n |n\rangle$. In this basis, the density operator is diagonal. Therefore, the density matrix of the thermal state becomes diagonal itself. From Equation (3.7), it follows that the distribution is unchanged during the protocol. By imposing the frictionless condition Equation (3.8) it can be concluded, that the basis of the Hamiltonian and the invariant are equal at initial and final times. Therefore, diagonal states expanded by the eigenbasis of the Hamiltonian will be diagonal in the eigenbasis of the invariant as well. By changing the frequency according to Equation (3.17), the system is initially in the state

$$\hat{\rho}(0) = \frac{e^{-\beta_0 \hat{H}(0)}}{\text{tr} \left[e^{-\beta_0 \hat{H}(0)} \right]}, \quad (3.23)$$

and will evolve to the final state

$$\hat{\rho}(t_f) = \frac{e^{-\beta_f \hat{H}(t_f)}}{\text{tr} \left[e^{-\beta_f \hat{H}(t_f)} \right]}, \quad (3.24)$$

where $\hat{H}(t_f)$ with $\omega(t_f) = \omega_f$ and a cooler/hotter inverse temperature $\beta_f = \gamma^2 \beta_0$.

3.4.3. Quantum dynamical evolution of Gaussian states

Coherent and thermal states are Gaussian states [Wee12]. Gaussian states are defined as such states, which have a Gaussian symmetric Wigner function $W(x)$.

$$W(\mathbf{x}) = W(q, p) = \frac{1}{\pi \hbar} \int_{-\infty}^{\infty} dy \langle q + y | \hat{\rho} | q - y \rangle e^{-\frac{i}{\hbar} p y} \quad (3.25)$$

The eigenvalues of the quadrature operator $\hat{\mathbf{x}} = (\hat{q}, \hat{p})$ are $\mathbf{x} = (q, p)$. Therefore, the first and the second-order moments have a one-to-one correspondence with the density operator $\hat{\rho} = \hat{\rho}(\bar{\mathbf{x}}, \mathbf{V})$ [Wee12]. $\bar{\mathbf{x}} = \langle \hat{\mathbf{x}} \rangle = \text{Tr}[\hat{\mathbf{x}} \hat{\rho}]$ is the first moment, which is often referred to as the displacement vector. \mathbf{V} denotes the covariant matrix, which has the entries $V_{ij} = \frac{1}{2} \langle \{ \Delta \hat{x}_i, \Delta \hat{x}_j \} \rangle$ with $\Delta \hat{x}_i = \hat{x}_i - \langle \hat{x}_i \rangle$ and $\{ \cdot, \cdot \}$ denotes the anti-commutator.

For Gaussian states of the harmonic oscillator, the statistic moments are constructed from the set of operators $\hat{\mathbf{X}} = \{ \hat{q}, \hat{p}, \hat{q}^2, \hat{p}^2, \hat{q}\hat{p} + \hat{p}\hat{q} \}$, which forms a closed Lie algebra, hence the Hamiltonian of a harmonic oscillator (3.9) is a linear combination of $\hat{\mathbf{X}}_i \in \hat{\mathbf{X}}$.

$$\hat{\mathbf{x}} = (\hat{q}, \hat{p}), \quad \mathbf{V} = \begin{pmatrix} \langle \hat{q}^2 \rangle - \langle \hat{q} \rangle^2 & \langle \hat{q}\hat{p} + \hat{p}\hat{q} \rangle - \langle \hat{q} \rangle \langle \hat{p} \rangle \\ \langle \hat{q}\hat{p} + \hat{p}\hat{q} \rangle - \langle \hat{q} \rangle \langle \hat{p} \rangle & \langle \hat{p}^2 \rangle - \langle \hat{p} \rangle^2 \end{pmatrix} \quad (3.26)$$

The Wigner function is expressed with first and second order statistical moments.

$$W(\mathbf{x}) = \frac{\exp \left[(\mathbf{x} - \bar{\mathbf{x}})^T \mathbf{V}^{-1} (\mathbf{x} - \bar{\mathbf{x}}) \right]}{2\pi \sqrt{\det \{ \mathbf{V} \}}} \quad (3.27)$$

\mathbf{V}^{-1} denotes the inverse matrix of \mathbf{V} and \mathbf{x}^T the transpose of \mathbf{x} . Hence $W(x)$ corresponds to the density operator and is constructed from operators $\hat{\mathbf{X}}_i \in \hat{\mathbf{X}}$, the use of wave packet propagation can be avoided. It is sufficient to evolve the expectation values $\bar{\mathbf{X}}_i(t) = \langle \hat{\mathbf{X}}_i(t) \rangle = \text{Tr}[\hat{\mathbf{X}}_i(t)\hat{\rho}(0)]$ in time using Equation (2.10), which simplifies in the Heisenberg picture to

$$\frac{d\bar{\mathbf{X}}_i}{dt} = \frac{i}{\hbar} [\hat{H}, \bar{\mathbf{X}}_i]. \quad (3.28)$$

The equation of motion is closed to the algebra as well. Therefore, a Gaussian state $\hat{\rho}(t)$ stays Gaussian during its evolution.

To evaluate the overlap between two states $\hat{\rho}_1$ and $\hat{\rho}_2$, the fidelity $\mathcal{F}(\hat{\rho}_1, \hat{\rho}_2) = \text{Tr}[\sqrt{\sqrt{\hat{\rho}_1}\hat{\rho}_2\sqrt{\hat{\rho}_1}}]$ [Nie09, p. 411] can be computed, using their respective first and second moments $\bar{\mathbf{x}}_1, \hat{\mathbf{V}}_1$ and $\bar{\mathbf{x}}_2, \hat{\mathbf{V}}_2$.

$$\mathcal{F}(\hat{\rho}_1, \hat{\rho}_2) = \mathcal{F}_0(\hat{V}_1, \hat{V}_2) \exp\left[-\frac{1}{4}\delta_{\bar{\mathbf{x}}}^T (\mathbf{V}_1 + \mathbf{V}_2)^{-1} \delta_{\bar{\mathbf{x}}}\right]. \quad (3.29)$$

$\delta_{\bar{\mathbf{x}}} = \bar{\mathbf{x}}_2 - \bar{\mathbf{x}}_1$ and $\mathcal{F}_0(\hat{V}_1, \hat{V}_2)$ is computed by

$$\mathcal{F}_0(\hat{V}_1, \hat{V}_2) = \frac{F_{\text{tot}}}{\sqrt[4]{\det(\hat{V}_1 + \hat{V}_2)}}, \quad (3.30)$$

with $F_{\text{tot}} = \sqrt[4]{\det\left[2\left(\sqrt{\hat{\mathbf{1}} + \frac{(\hat{V}_{\text{aux}}\hat{\Omega})^{-2}}{4}} + \hat{\mathbf{1}}\right)\hat{V}_{\text{aux}}\right]}$. \hat{V}_{aux} is an auxiliary matrix, obtained from

$$\hat{V}_{\text{aux}} = \hat{\Omega}^T (\hat{V}_1 + \hat{V}_2)^{-1} \left(\frac{\hat{\Omega}}{4}\hat{V}_2\hat{\Omega}\hat{V}_1\right), \quad (3.31)$$

with $\hat{\Omega} = \begin{pmatrix} 0 & 1 \\ -1 & 0 \end{pmatrix} \otimes \hat{\mathbf{1}}$ [Ban15].

4. Numerical methods

4.1. Strömer-Verlet method

Many methods are developed to propagate a classical trajectory [Sin10]. A very stable numerical method for integrating time dependence is the so called Strömer-Verlet method [Hai03]. In this method, the dynamical variables are partitioned into two groups, which are propagated by two *different* Runge-Kutta methods. In general the dynamical variables are position \vec{r} and velocity \vec{v} . As an example a classical non-relativistic particle of mass m and charge q is used. The Hamiltonian of such a particle in an arbitrary conservative electric potential $V(\vec{r}, t)$ has the general form:

$$H(\vec{r}, \vec{v}, t) = \frac{m}{2} |\vec{v}|^2 + V(\vec{r}, t). \quad (4.1)$$

By expressing the canonical equations as finite differences, the equation of motion can be derived.

$$\vec{r}_{n+1} - 2\vec{r}_n + \vec{r}_{n-1} = -dt^2 \frac{q}{m} \nabla V(\vec{r}_n, t_n). \quad (4.2)$$

Here dt denotes the length of one time step. The issue here is, that x_{-1} is unknown. The canonical equations yields:

$$\frac{1}{m} \nabla_{\vec{v}} H(\vec{r}, \vec{v}, t) = \vec{v} = \frac{d\vec{r}}{dt}. \quad (4.3)$$

The velocity can be rewritten as symmetric finite difference, by expressing the time derivative of the position as finite difference

$$\vec{v}_n = \frac{\vec{r}_{n+1} - \vec{r}_{n-1}}{2\Delta t}, \quad (4.4)$$

with Δt denoting the finite time step. For a tolerable error ϵ the step size is best chosen to be $\Delta t = \sqrt{\epsilon}$ to obtain the best compromise between accumulated floating point errors and numerical errors. By using the initial position \vec{x}_0 and initial velocity \vec{v}_0 , \vec{x}_{-1} can be eliminated. This yields for \vec{r}_1 :

$$\vec{x}_1 = \vec{x}_0 + \Delta t \vec{v}_0 + \frac{\Delta t^2}{2} \frac{q}{m} \nabla V(\vec{r}_n, t_n) \quad (4.5)$$

For further propagation, the following recursion relations are used

$$\vec{v}_{n+\frac{1}{2}} = \vec{v}_n + \frac{\Delta t}{2} \frac{q}{m} \nabla V(\vec{r}_n, t_n) \quad (4.6)$$

$$\vec{r}_{n+1} = \vec{r}_n + \Delta \vec{v}_{n+\frac{1}{2}} \quad (4.7)$$

$$\vec{v}_{n+1} = \vec{v}_{n+\frac{1}{2}} + \frac{\Delta t}{2} \frac{q}{m} \nabla V(\vec{r}_n, t_n). \quad (4.8)$$

If one is not interested in \vec{v}_{n+1} , Equation (4.8) can be inserted in Equation (4.6), to obtain

$$\vec{v}_{n+\frac{1}{2}} = \vec{v}_{n-\frac{1}{2}} + \frac{\Delta t}{2} \frac{q}{m} \nabla V(\vec{r}_n, t_n). \quad (4.9)$$

Example source code can be found in Appendix A.1.

4.2. Gradient ascent/descent method

The gradient descent method is a powerful tool to maximize/minimize a control functional with respect to a certain parameter. For example it can be utilized to maximize/minimize friction in a problem with dissipation.

The dynamic of a density operator $\hat{\rho}(t)$ is obtained from the Liouville equation (2.16)

$$\dot{\hat{\rho}}(t) = \frac{i}{\hbar} \left[\hat{\rho}(t), \hat{H}_0 + \sum_{\ell} \xi_{\ell}(t) \hat{H}_{\ell} \right]. \quad (4.10)$$

\hat{H}_0 denotes the time-independent Hamiltonian of the system and \hat{H}_{ℓ} describes the control field, which have the time-dependent amplitudes $\xi_{\ell}(t)$. Furthermore, the control vector is defined as $\xi(t) \equiv (\xi_1(t), \xi_2(t), \dots, \xi_L(t))$ [Kha05]. To find the optimal amplitudes $\xi_{\ell}(t)$ to transfer from the initial state $\hat{\rho}(t_0 := 0)$ to a target state $\hat{\rho}_{\text{tar}}$ at the final time t_f . For hermitian $\hat{\rho}_{\text{tar}}$ and $\hat{\rho}(t_f)$ the performance index is defined as

$$\Phi_0 = \langle \hat{\rho}_{\text{tar}}, \hat{\rho}(t_f) \rangle_{\text{HS}} = \text{Tr}[\hat{\rho}_{\text{tar}} \hat{\rho}(t_f)]. \quad (4.11)$$

A more general approach to obtain the performance index can be found in [Kha05] and [Goe15]. By discretising the interval in N equal spaced steps $\Delta t = \frac{t_f}{N}$, the time evolution operator after the j -th step takes the form

$$\hat{U}_j = \exp \left[-\Delta t \left(\hat{H}_0 + \sum_{\ell} u_{\ell}(j) \hat{H}_{\ell} \right) \right]. \quad (4.12)$$

The performance index takes the form

$$\Phi_0 = \left\langle \hat{\rho}_{\text{tar}}, \hat{U}_N \dots \hat{U}_1 \hat{\rho}(0) \hat{U}_1^{\dagger} \dots \hat{U}_N^{\dagger} \right\rangle_{\text{HS}} = \text{Tr} \left[\hat{\rho}_{\text{tar}} \hat{U}_N \dots \hat{U}_1 \hat{\rho}(0) \hat{U}_1^{\dagger} \dots \hat{U}_N^{\dagger} \right] \quad (4.13)$$

Hence the Hilbert-Schmidt product is invariant under cyclic permutation, Equation (4.13) is equivalent to

$$\Phi_0 = \left\langle \underbrace{\hat{U}_{j+1}^{\dagger} \dots \hat{U}_N^{\dagger} \hat{\rho}_{\text{tar}} \hat{U}_N \dots \hat{U}_{j+1}}_{=\hat{\rho}_{\text{tar}}^{(j)}}, \underbrace{\hat{U}_j \dots \hat{U}_1 \hat{\rho}(0) \hat{U}_1^{\dagger} \dots \hat{U}_j^{\dagger}}_{=\hat{\rho}^{(j)}} \right\rangle_{\text{HS}}. \quad (4.14)$$

The density operator at time $t = j\Delta t$ is can be expressed as $\hat{\rho}(t) = \hat{\rho}^{(j)}$ and $\hat{\rho}_{\text{tar}}^{(j)}$ is the target state which is propagated backwards at the same time. The derivative of the performance index is derived in [Kha05]

$$\frac{\delta \Phi_0}{\delta \xi_{\ell}(j)} = -\frac{i}{\hbar} \left\langle \hat{\rho}_{\text{tar}}^{(j)}, \Delta t \left[\hat{H}_{\ell}, \hat{\rho}^{(j)} \right] \right\rangle_{\text{HS}} \quad (4.15)$$

To obtain the maximum or minimum of the performance index the control field needs to be updated. In the case of maximization, the derivative of the performance index with respect to the control amplitude is added with a sufficiently small factor $\mu > 0$ to the old control amplitude. In the case of minimization, the derivative is subtracted.

$$\xi_\ell(j) \rightarrow \xi_\ell(j) \pm \mu \frac{\delta\Phi_0}{\delta\xi_\ell(j)}. \quad (4.16)$$

This method can be used for pulse optimization and is then referred to as gradient ascend pulse engineering (GRAPE) [Kha05]. The steps needed for an implementation are depicted in Figure 4.1.

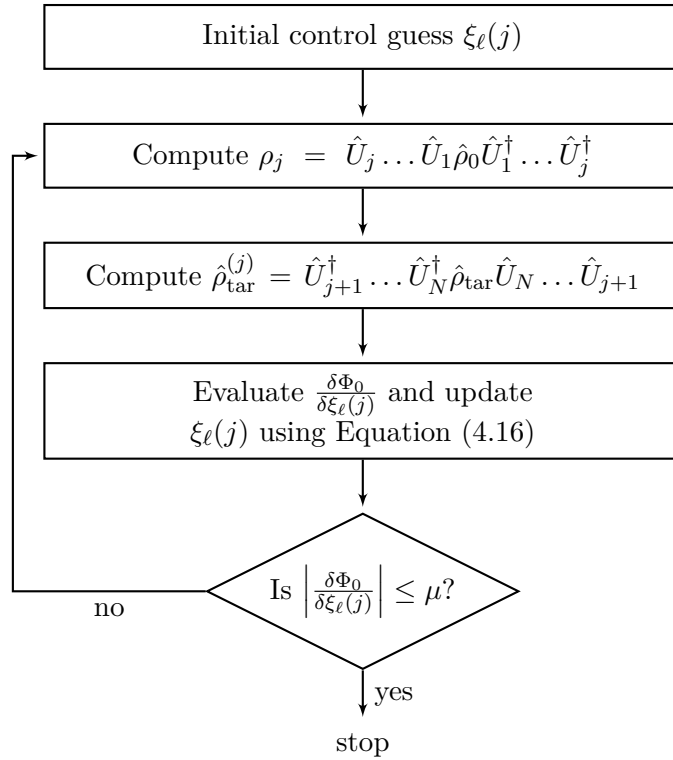


Figure 4.1.: Flowchart for implementing GRAPE.

This protocol is employed, when the dimension of the control vector is large. Since only two full time propagations are needed, it can be much faster than a conventional implementation to obtain the gradient $\delta\Phi_0/\delta\xi_\ell(j)$. Therefore, this method is well-suited for the optimization of for example nuclei magnetic resonance pulse sequences. Another advantage of this method is that the pulses can be truly arbitrary and the orders of magnitudes of the amplitudes can be much higher compared to other optimization schemes.

However, this method does not yield a fast convergence. To obtain faster convergences, Newton's method can be implemented. For that the second derivative needs to be computed. The second derivative is generally obtained from the Hessian matrix $\mathbf{H}^{(j)}$ with entries

$$\mathbf{H}_{a,b}^{(j)} = \frac{\delta^2\Phi_0}{\delta\xi_a(j)\delta\xi_b(j)}. \quad (4.17)$$

However the computation of the full Hessian matrix is expensive. Therefore, the Hessian is estimated with help of available information from $\frac{\delta\Phi_0}{\delta\xi_\ell(j)}$. Such schemes are called quasi-Newton methods [Goe15].

4.2.1. Reduction of radio frequency power and limited radio frequency amplitudes

In experiments, high radio frequency powers are often not feasible to implement. This is especially true for pulse engineering, since the modulation needs to be much lower than the frequency it self. Furthermore, radio frequency amplitudes are only available in limited ranges and radio frequency amplitudes lead to thermal noise due to heating. To obtain a lower and a more accessible control amplitude, the previously described method can be applied. By penalizing high amplitudes, the performance function takes the form

$$\Phi_{\text{RF}} = a \sum_{k=1}^N \sum_{\ell}^L \xi_\ell^2(j) \Delta t, \quad (4.18)$$

with a is the weight of the penalty for high rf-powers. The gradient takes the form

$$\frac{\delta\Phi_{\text{RF}}}{\delta\xi_\ell(j)} = -2a\xi_\ell(j)\Delta t. \quad (4.19)$$

When the maximal available amplitude ξ_{max} is exceeded, the amplitude $\xi_\ell(j)$ is set to ξ_{max} , when updating the amplitudes. Therefore, the algorithm depicted in Figure 4.1 can still be applied.

4.2.2. Robustness

To obtain higher stability in an implementation, it is crucial to find the optimal performance under the influence of experimental imperfections. For a range of parameters ζ , which account for radio frequency miscalibration and radio frequency inhomogeneity for a range of radio frequency amplitudes, this method can also be used. If this set is sampled over finite elements ζ_p , the performance function is obtained as the sum over these finite elements. Assuming the population transfer is hermitian, as in 4.2, the performance function is obtained as [Kha05]

$$\Phi_{\text{tot}} = \sum_p \left\langle \hat{\rho}_{\text{tar}}^{(j)}(\zeta_p), \hat{\rho}^{(j)}(\zeta_p) \right\rangle_{\text{HS}} \quad (4.20)$$

with the derivative

$$\frac{d\Phi_{\text{tot}}}{d\xi_\ell(j)} = -\frac{i}{\hbar} \sum_p \left\langle \hat{\rho}_{\text{tar}}^{(j)}(\zeta_p), \Delta t \left[\hat{H}_\ell, \hat{\rho}^{(j)}(\zeta_p) \right] \right\rangle_{\text{HS}}. \quad (4.21)$$

This method can also implemented for other noise sources, like chemical shifts in a sample or other experimental imperfections.

5. Results

In this chapter, invariant-based reverse engineering is applied to a trapped ion to obtain a speed-up in an adiabatic expansion/compression. By allowing non-confining potentials for a short period of time, much faster processes can be obtained.

Most of the presented results have been published in:

Transient Non-Confining Potentials for Speeding Up a Single Ion Heat Pump, E. Torrontegui, S. T. Dawkins, M. Göb, K. Singer, *New Journal of Physics* **20**, 105001 (2018).

5.1. Proposed experimental implementation

To implement a shortcut to adiabaticity a common voltage will be applied to the end-caps. The radio frequency voltages on the rod electrodes will be switched off. This is necessary, because the radio frequency voltage can only be modulated more slowly than the its frequency of the radio drive. Furthermore, in the tapered design, the radio frequency potentials lead to a coupling between the radial and axial degrees of freedom. Switching off the radio frequency driven radial confinement requires a solid state radio frequency toggle switch [Tan09] in front of a high voltage radio frequency generator [Jon97]. More recent setups employ a low voltage radio frequency power supply connected to subsequent radio frequency amplifier with $50\ \Omega$ impedance instead off a high voltage radio frequency generator. The impedance of the ion trap itself is matched using the inductive coupling of a helical resonator [Siv12]. To avoid reflections, the power needs to be feed to a dump with the same impedance as the radio frequency trapping electrodes of the ion trap. This is depicted in 5.1.

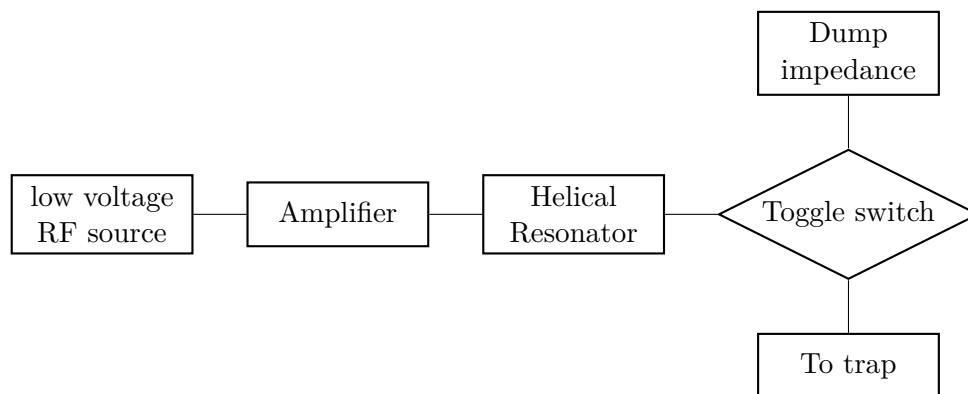


Figure 5.1.: Schematic for fast switching off rf voltages to the trap electrodes.

To implement the shortcut protocol in a linear Paul trap without taper (see Figure 1.1), it is sufficient to lower the amplitude during the shortcut, hence axial and radial direction are not coupled by the oscillating saddle potential.

The 3D-Hamiltonian of an ion trapped in a confining potential of a Paul trap (Section 1.2.1), supplied by symmetric driven rf voltages and dc voltages on the end-caps reads

$$\hat{H} = \frac{\hat{\mathbf{p}}^2}{2m} + \frac{m}{2} [\Omega(t) + \Delta(t)]^2 + \hat{x}^2 + \frac{m}{2} [\Omega(t) + \Delta(t)]^2 + \hat{y}^2 + \frac{m}{2} \omega_z^2(t) \hat{z}^2, \quad (5.1)$$

with $\hat{\mathbf{p}} = (\hat{p}_x, \hat{p}_y, \hat{p}_z)$, $\omega_z(t)$ the trapping frequency in axial direction and $\omega_r(t) = \omega_x(t) = \omega_y(t) = \Omega(t) + \Delta(t)$ the trapping frequencies in radial directions, which are composed of a combination of radio frequency and dc voltages. It is important to keep in mind that the resulting trapping frequency is not obtained by simply adding the frequencies of the pseudo potential and the direct current potential. Especially, when large voltages are involved. For further insight, see [Lei03].

The ion is symmetrically confined in the x - y plane. The energy of these two degrees of freedom are used as the working agent. The degree of freedom in the axial direction is considered as classical piston, which is driven by the working agent. Furthermore, the axial degree of freedom can be neglected, because the ion is held at the minimum of the confinement in z -direction. Because of the radial symmetry, the radial terms in Equation (5.1) reads

$$\hat{H}_r = \frac{\hat{p}_r^2}{2m} + \frac{1}{2} m \omega_r^2(t) \hat{r}^2, \quad (5.2)$$

with $\hat{p}_r^2 = \hat{p}_x^2 + \hat{p}_y^2$ and $\hat{r}^2 = \hat{x}^2 + \hat{y}^2$. It comes to notice, that the radial Hamiltonian \hat{H}_r has the same structure as in Equation (3.9). Because of this, the trapping frequency can be changed from $\omega_r(0) = \omega_{r,0}$ to $\omega_r(t_f) = \omega_{r,t_f}$ by using the invariant-based reverse engineering approach, which is described in Section 3.3. A shortcut to adiabaticity protocol $\omega^2(t) = \frac{\omega_{r,0}}{b_r^4(t)} - \frac{\ddot{b}_r(t)}{b_r(t)}$ can be reverse-engineered, with the free function $b_r(t)$ satisfying the frictionless boundary conditions (Equation (3.8)). The compression/expansion ratio reads $\gamma_r = \sqrt{\omega_{r,0}/\omega_{r,t_f}}$.

5.2. Robustness improvements

The control of fast changing voltages is prone to errors. To make the shortcut protocol as resilient to noise as possible, gradient descent methods are employed to reduce the employed power (4.2.1). This leads to an improved heat extraction process with the optimized protocol, since the main source of imperfections is the time variation of $\omega^2(t)$. The largest limitations are the slew rate and bandwidth limitation of digital-to-analog converters. Therefore, a slow change in $\omega^2(t)$ is desired. Due to the freedom in constructing the protocol during the shortcut additional constraints can be implemented. For example, $d\omega^2(t)/dt = \partial_t(\omega^2(t))$ can be minimized to consider these experimental constraints.

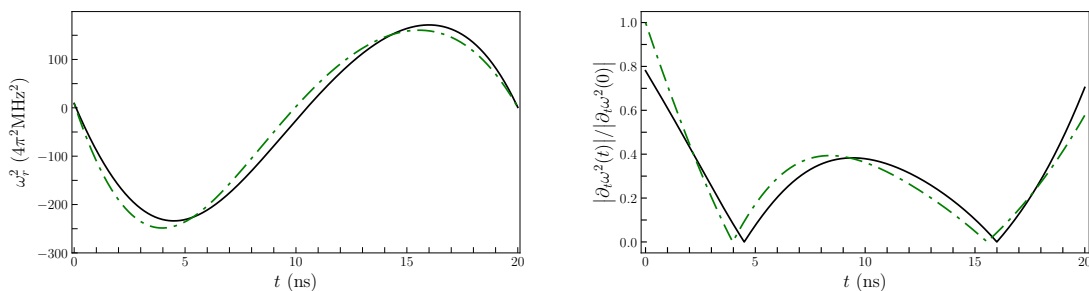
Minimizing the power needed to perform the shortcut will improve the heat extraction process. Therefore, the maximal absolute value of the derivative of the control

with respect to time in the interval $t \in [0, t_f]$, $\max |\partial_t(\omega^2(t))|$, needs to be minimized. The trivial solution is obtained for $\partial_t(\omega^2(t)) = 0$, which yields the control $\omega_{\text{uopt}}^2(t) = \text{const}$. This violates the boundary conditions (3.12) and is therefore, not a physical solution. Furthermore, this control does not yield a change in frequency and is therefore not suitable to perform such a change. Under the assumption that $\omega^2(t)$ is continuous over the closed interval $[0, t_f]$ and differentiable over the open interval $(0, t_f)$, the mean value theorem yields a useful bound. For $\omega^2(0) = \omega_0^2$ and $\omega^2(t_f) = \omega_{t_f}^2$, the absolute maximum of $\partial_t(\omega^2(t))$ needs to be

$$\frac{d\omega^2(t)}{dt} \geq \frac{\omega_0^2 - \omega_{t_f}^2}{t_f}. \quad (5.3)$$

The equality holds for the linear control $\omega^2(t) = \omega_0^2 + (\omega_0^2 - \omega_{t_f}^2) t/t_f$. The free function $b(t)$, obtained by Equation (3.17), violates the imposed boundary conditions (3.12). Instantaneous switching would be needed to implement such a control, due to discontinuities in $\dot{b}(t)$ and $\ddot{b}(t)$ at $t = 0$ and t_f . This is often not experimentally feasible, especially in short time frames.

The free function has a non-unique solution to fulfill the frictionless boundary conditions. Exploiting this fact, the function can be expanded to a higher order, which yields additional parameters a_i [Lev17; Lev18]. Due to this additional parameter the $\omega^2(t, a_i)$ can be optimized using the gradient descent method to obtain the optimal solution $\omega_{\text{opt}}^2(t, a_i)$.



(a) Optimized and standard control $\omega^2(t)$. (b) Relative time derivatives of the control.

Figure 5.2.: The shortcut protocol constructed with a standard 6-th order interpolation (green dashed line) and the control with additional parameter (black solid line) are visualized in 5.2a and their respective time derivatives in 5.2b.

To demonstrate this, an expansion from $\omega(0)/2\pi = 3$ MHz to $\omega(t_f)/2\pi = 1$ MHz over the time of $t_f = 20$ ns was constructed. A reduction of $\max |\partial_t(\omega_{\text{opt}}^2(t))| / \max |\partial_t(\omega^2(t))| \sim 0.78$ is obtained by expanding $b(t)$ to the 6-th order.

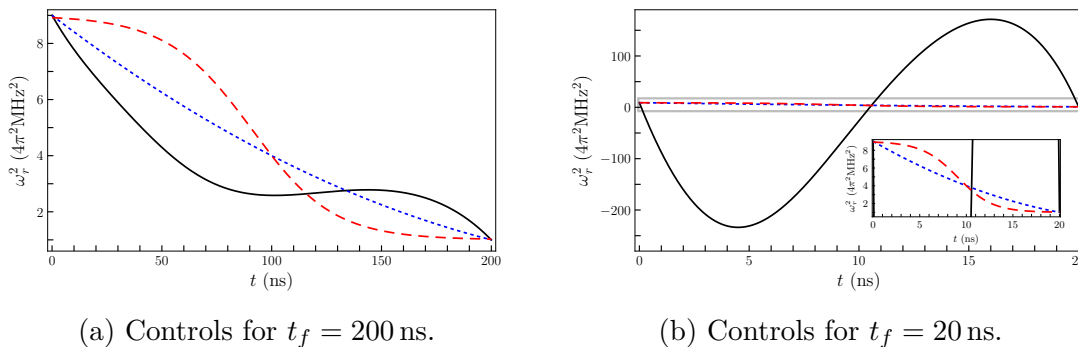
5.3. STA in comparison

To compare the performance, the STA protocol is compared to the linear protocol, which is derived in Section 5.2, and the smooth ramp protocol. The smooth ramp

protocol reads

$$\omega(t) = \frac{\omega_0 e^{\Gamma t_0} + \omega_f e^{\Gamma t}}{e^{\Gamma t_0} + e^{\Gamma t}}, \quad (5.4)$$

where Γ denotes the slope of the ramp. An expansion from $\omega_0/2\pi = 3$ MHz to $\omega_f/2\pi = 1$ MHz over a time of $t_{f1} = 200$ ns and $t_{f2} = 20$ ns. The three protocols are depicted in Figure 5.3.



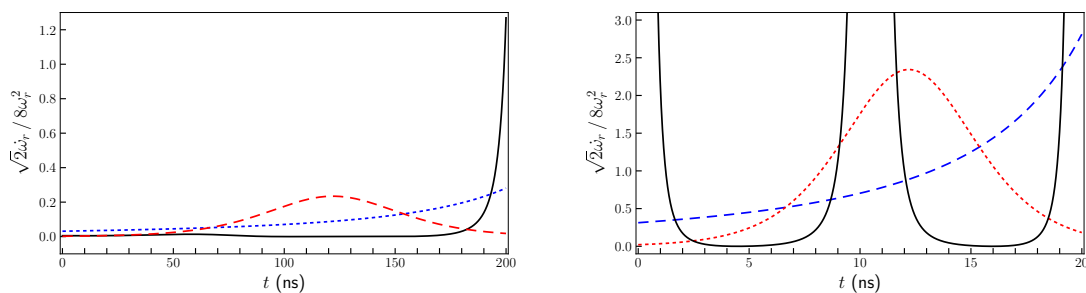
(a) Controls for $t_f = 200$ ns.

(b) Controls for $t_f = 20$ ns.

Figure 5.3.: The shortcut protocol (black solid), the linear ramp (blue dotted) and the smooth ramp (red dashed) in comparison for a duration of 200 ns (a) and 20 ns (b). The inset in (b) shows a higher detailed view of the area with the grey rectangle.

Already for a duration of 200 ns, it is not feasible to implement the presented shortcut protocol using amplitude modulation. Hence the duration is in the order of one period with typical frequencies $\Omega_{\text{rf}}/2\pi \sim 20$ MHz. Therefore, the effective trapping frequency in radial directions needs to be modulated by supplying voltages to the cap electrodes. By allowing negative ω^2 as well, a significant speed up of one order of magnitude is obtained. These negative squared frequency corresponds to a non-confining potential, which can be also applied by ramping the dc voltage on the cap electrodes. The feasibility of such transient non-confining potentials is further discussed in Section 5.4.

Furthermore, it is of particular interest to examine the adiabaticity parameter μ (3.2) of the presented protocols. These are presented in Figure 5.4.



(a) Adiabaticity coefficient for $t_f = 200$ ns.

(b) Adiabaticity coefficient for $t_f = 20$ ns.

Figure 5.4.: The adiabaticity coefficient of the shortcut protocol (black solid), the linear ramp (blue dotted) and the smooth ramp (red dashed) in comparison for a duration of 200 ns (a) and 20 ns (b).

The STA protocol leads to a clear non-adiabatic behavior. In Figure 5.4a it comes to notice, that approaching t_f the adiabaticity parameter diverges. It becomes even clearer in Figure 5.4b. Here, the adiabaticity parameter diverges at 10 ns, due to the zero crossing of $\omega^2(t)$. Even though this protocols are not adiabatic, they still lead to a transfer without unwanted excitations.

5.3.1. Fidelity evaluation

To verify that the shortcut protocol indeed provides a super-adiabatic drive, the overlap to the target state $\hat{\rho}_{\text{tar}}$ needs to be evaluated. Therefore, the fidelity $\mathcal{F}(\hat{\rho}(t_f), \hat{\rho}_{\text{tar}})$ (3.30) is computed for all three presented protocols in dependence of the duration of the protocol t_f .

A thermal state with initial inverse temperature β_0 described by the Hamiltonian $\hat{H}(0)$ with frequency $\omega_{r,0}$ is fully characterized by its statistical moments $\bar{\mathbf{X}}(0)_1 = \bar{\mathbf{X}}(0)_2 = \bar{\mathbf{X}}(0)_5 = 0$,

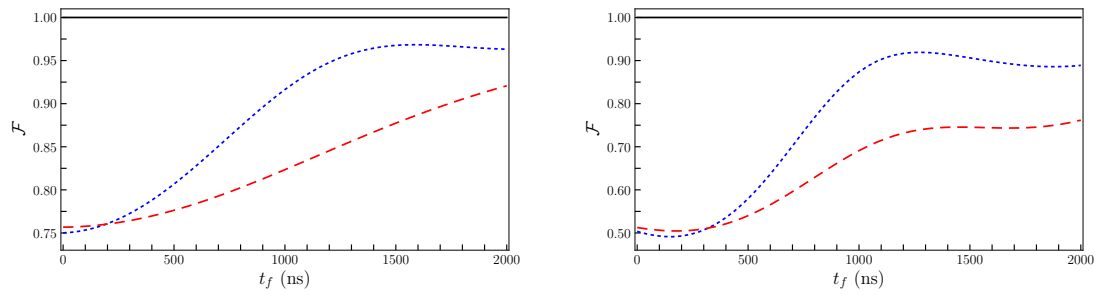
$$\bar{\mathbf{X}}_3(0) = l_0^2 \coth\left(\frac{\beta_0 \hbar \omega_{r,0}}{2}\right) \quad \text{and} \quad \bar{\mathbf{X}}_4(0) = k_0^2 \coth\left(\frac{\beta_0 \hbar \omega_{r,0}}{2}\right), \quad (5.5)$$

with $l_0 = \sqrt{\frac{\hbar}{2m\omega_{r,0}}}$ and $k_0 = \sqrt{\frac{\hbar m \omega_{r,0}}{2}}$. The target state has an inverse temperature $\beta_f = \gamma_r^2 \beta_0$ at a final frequency ω_{r,t_f} with similar statistical moments. The fidelity of the three protocols with an initial thermal state is depicted in Figure 5.5a. As depicted in Figure 5.5a, the invariant-based reverse engineered control has a fidelity of 1 by construction, independent of the final time t_f .

In analogy to the thermal states, the fidelity of the three presented protocols is examined for coherent states. The initial statistical moments read

$$\begin{aligned} \bar{\mathbf{X}}_1(0) &= 2l_0 \operatorname{Re}(\alpha_0), & \bar{\mathbf{X}}_2 &= 2k_0 \operatorname{Im}(\alpha_0), \\ \bar{\mathbf{X}}_3(0) &= \bar{\mathbf{X}}_1^2(0) + l_0^2, & \bar{\mathbf{X}}_4(0) &= \bar{\mathbf{X}}_2^2(0) + k_0^2, \quad \text{and} \quad \bar{\mathbf{X}}_5(0) = 4\hbar \operatorname{Re}(\alpha_0) \operatorname{Im}(\alpha_0). \end{aligned} \quad (5.6)$$

They correspond to $\hat{H}(0)$ and $\omega_{r,0}$. The displacement parameter of the target state $\alpha_f = \alpha_0 e^{-ig\omega_{r,0}}$ with $g = \int_0^{t_f} d\tau / b(t)^2$ at $\hat{H}(t_f)$. The initial displacement parameter was chosen $\alpha_0 = 1 + i$. The fidelity of the three compared protocols is depicted in Figure 5.5b. The shortcut to adiabaticity protocol leads again to a fidelity of 1 by construction.



(a) Initial thermal states.

(b) Initial coherent states.

Figure 5.5.: Fidelity of the shortcut protocol (black solid), the linear ramp (blue dotted) and the smooth ramp (red dashed) in dependence of the final time t_f with an initial thermal state (a) and an initial coherent state (b).

5.4. Confirmation of trapping condition

As seen in Section 5.3.1, the shortcut has by construction a fidelity of 1 even at short durations. But this does not guarantee stable trapping conditions during the transient non-confining period. Therefore, the position of the ion in the x - y plain was simulated, using the Strömer-Verlet method, which is described in Section 4.1 and a minimal example for a three-dimensional harmonic oscillator is found in Appendix A.1.

In this simulation, the acceleration was computed from the analytic formula (1.5), therefore also accounting for micromotion. The initial parameters were chosen randomly from a Gaussian distribution with a mean value of zero and a variance of $\sqrt{k_B T/m}$, with the Boltzmann constant k_B and temperature $T = 2$ mK. From these initial parameter, the position and velocity were propagated for a whole period, before the shortcut protocol (Figure 5.6a) or the linear ramp (Figure 5.6b) was applied with a duration of $t_f = 20$ ns.

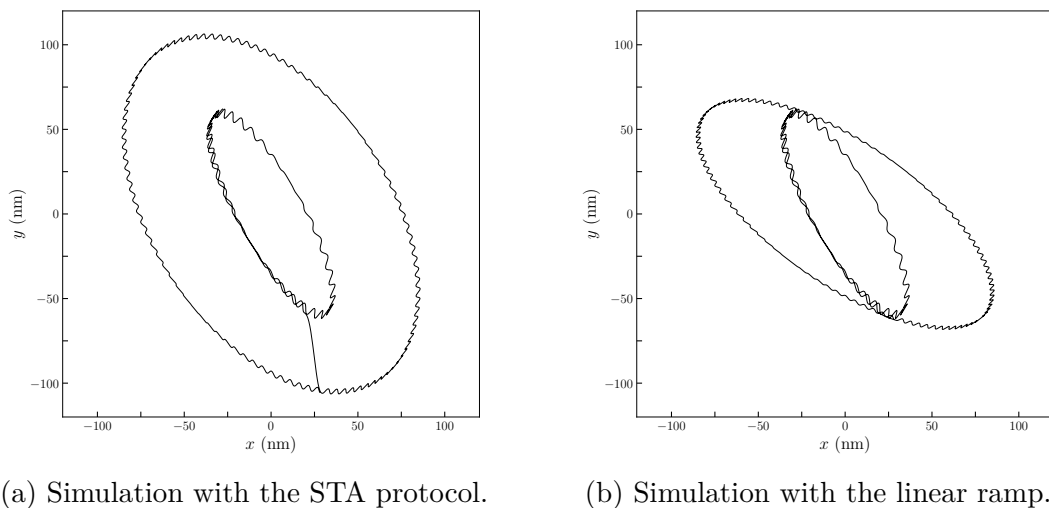


Figure 5.6.: Simulated trajectories of an ion under the influence of the shortcut protocol (a) and the linear ramp (b).

Both protocols yield stable trapping conditions. The shortcut to adiabaticity yields a phase relation preserving drive, which with the linear ramp drive the ion is excited. This excitation leads to a rotation of the ion's elliptical trajectory. As observed, the shortcut to adiabaticity protocol leads to stable trapping condition even with non-confining potentials for a brief duration. Thus it is feasible to implement experiment, hence the ion is trapped after the super adiabatic expansion/compression. Though this method requires sophisticated electronics to allow for a fast and precise control of the radio frequency voltages, which are required to perform the shortcut.

6. Outlook

In conclusion, the proposed protocol can be utilized to speed up adiabatic processes for trapped ions, yielding an ultra-fast and high-fidelity compression/expansion process. The use of transient non-confining potentials enables an even higher speed up. By optimizing the protocol, a lower power to perform the shortcut is obtained, leading to lower noise on the control and therefore a more efficient heat pump. This protocol can be utilized in Otto cycle based heat engines and refrigerators. The cycle time can be drastically reduced, which gives rise to the power of the engine. By implementing a quantum Otto heat engine [Kos17] into the experimental system of the single-atom heat engine, more underlying questions can be studied. Furthermore, finite time thermalization processes can be investigated in the presented set up. By implementing shortcuts to equilibration (STE) [Dan19b] or discrete isothermal process (DIP) [Ma18], a Stirling engine with a single atom running at a finite time can be realized. These stroke heat engines/refrigerators [Kos84] yield a toolbox for to approach absolute zero temperature [Tor13a] and for testing thermodynamic laws at a single particle level. The presented expansion/compression protocol can be utilized for heat engines/refrigerators with continuous bath contact [Kos14].

6.1. Single-atom heat engine as sensible quantum heat probe

The single-atom heat engine operates between two baths. By examining the work output of the engine, operating with one known and one unknown bath, it is possible to characterize the unknown bath.

Due to the coupling of axial and radial direction, work is flowing in the axial direction, increasing the amplitude of the oscillation. The growth of the amplitude $d\Delta z/dt$ is linear and solely dependent on the difference in temperature of ΔT . The first numerical results confirmed the analytic model.

A. Appendix

A.1. Implementation of the Strömer-Verlet method

In this chapter, an implementation of the Strömer-Verlet method is presented. As an example we will use a harmonic potential which confines a particle in three dimension. The acceleration can be calculated by simply taking minus the derivative of the potential with respect to the coordinate and divide it by the mass.

```
1 #include <iostream>
2 #include <fstream>
3 #include <limits>
4 #define _USE_MATH_DEFINES
5 #include <math.h>
6
7 void stroemerVerlet(double * oldPos, double * oldVel, double * omega,
8     double dt, int dim, double * newPos, double * newVel) {
9     double * velHalf = new double[dim];
10    for (int i = 0; i < dim; ++i) {
11        velHalf[i] = oldVel[i] + dt / 2.0*(-omega[i]*omega[i]*oldPos[i]);
12    }
13    for (int i = 0; i < dim; ++i) {
14        newPos[i] = oldPos[i] + dt * velHalf[i];
15    }
16    for (int i = 0; i < dim; ++i) {
17        newVel[i] = velHalf[i]+dt / 2.0*(-omega[i] * omega[i] * newPos[i]);
18    }
19    delete[] velHalf;
20 }
21
22 int main(int argc, char ** argv) {
23
24     double finalTime = 1e-5;
25     double dt = sqrt(std::numeric_limits<double>::epsilon()*finalTime);
26     int steps = static_cast<int>(finalTime / dt);
27     std::cout << steps << std::endl;
28
29     //allocate array for position and velocity
30     double ** position = new double*[steps];
31     double ** velocity = new double*[steps];
32     for (int i = 0; i < steps; ++i) {
33         position[i] = new double[3];
34         velocity[i] = new double[3];
35     }
36     double * velHalf = new double[3];
37
38     //set initial conditions
```

```

39 position[0][0] = 1.0e-6;
40 position[0][1] = -1.0e-6;
41 position[0][2] = 1.0e-6;
42 velocity[0][0] = 0.0e-6;
43 velocity[0][1] = 0.0e-6;
44 velocity[0][2] = 0.0e-6;
45
46 //set frequency
47 double omega[3];
48 omega[0] = 2*M_PI*1.0e6;
49 omega[1] = 2 * M_PI*1.0e6;
50 omega[2] = 2 * M_PI*0.1e6;
51
52 for (int i = 1; i < steps; ++i) {
53     stroemerVerlet(position[i - 1], velocity[i - 1], omega, dt,3,
54     position[i], velocity[i]);
55     if (!(i % 100)) std::cout << i << " / " << steps << std::endl;
56 }
57
58 std::ofstream results;
59 results.open("results.txt");
60 for (int i = 0; i < steps; ++i) {
61     results << i * dt << '\t' << position[i][0] << '\t' << position[i]
62     ][1] << '\t' << position[i][2] << '\t' << velocity[i][0] << '\t' <<
63     velocity[i][1] << '\t' << velocity[i][2] << std::endl;
64 }
65
66 results.close();
67 std::cin.get();
68 return 0;
69 }

```

In Figure A.1 the result of this example is depicted.

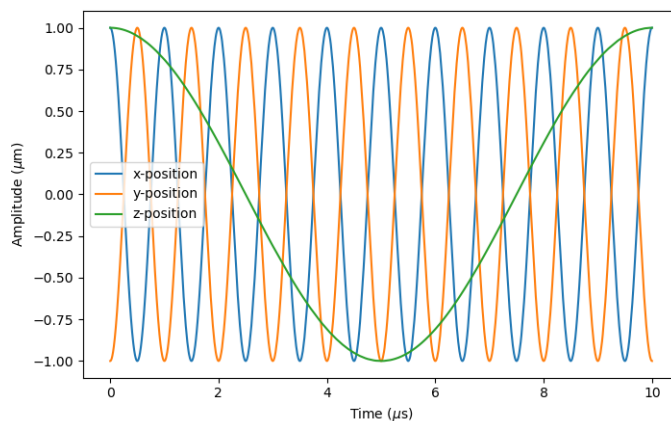


Figure A.1.: Movement of an particle in a three-dimensional harmonic potential.

B. List of publications

The following article has been published during the preparation of this thesis.

Transient Non-Confining Potentials for Speeding Up a Single Ion Heat Pump

E. Torrontegui, S. T. Dawkins, M. Göb, K. Singer
New Journal of Physics **20**, 105001 (2018).

We propose speeding up a single ion heat pump based on a tapered ion trap. If a trapped ion is excited in an oscillatory motion axially the radial degrees of freedom are cyclically expanded and compressed such that heat can be pumped between two reservoirs coupled to the ion at the turning points of oscillation. Through the use of invariant-based inverse engineering, we can speed up the process without sacrificing the efficiency of each heat pump cycle. This additional control can be supplied with additional control electrodes or it can be encoded into the geometry of the radial trapping electrodes. We present novel insight how speed up only limited by the magnitude of the control voltage can be achieved through the use of inverted harmonic potentials. We have verified that stable trapping conditions can be achieved.

Bibliography

- [Aba19] O. Abah and M. Paternostro, “Shortcut-to-adiabaticity Otto engine: A twist to finite-time thermodynamics”, *Physical Review E* **99**, 022110 (2019).
- [Bae09] H. D. Baehr and S. Kabelac, “Thermodynamik: Grundlagen und technische Anwendungen (Springer-Lehrbuch) (German Edition)”, Springer (2009).
- [Ban15] L. Banci, S. L. Braunstein, and S. Pirandola, “Quantum Fidelity for Arbitrary Gaussian States”, *Physical Review Letters* **115**, 260501 (2015).
- [Bea16] M. Beau, J. Jaramillo, and A. del Campo, “Scaling-Up Quantum Heat Engines Efficiently via Shortcuts to Adiabaticity”, *Entropy* **18**, 168 (2016).
- [Ben00] C. M. Bender, D. C. Brody, and B. K. Meister, “Quantum mechanical Carnot engine”, *Journal of Physics A: Mathematical and General* **33**, 4427 (2000).
- [Ber98] D. J. Berkeland, J. D. Miller, J. C. Bergquist, W. M. Itano, and D. J. Wineland, “Minimization of ion micromotion in a Paul trap”, *Journal of Applied Physics* **83**, 5025 (1998).
- [Bre19] S. M. Brewer, J.-S. Chen, A. M. Hankin, E. R. Clements, C. W. Chou, D. J. Wineland, D. B. Hume, and D. R. Leibbrandt, “ $^{27}\text{Al}^+$ Quantum-Logic Clock with a Systematic Uncertainty below 10^{-18} ”, *Physical Review Letters* **123**, 033201 (2019).
- [Bro86] L. S. Brown and G. Gabrielse, “Geonium theory: Physics of a single electron or ion in a Penning trap”, *Reviews of Modern Physics* **58**, 233 (1986).
- [Çak19] B. Çakmak and Ö. E. Müstecaplı, “Spin quantum heat engines with shortcuts to adiabaticity”, *Physical Review E* **99**, 032108 (2019).
- [Cal85] H. B. Callen, “Thermodynamics and an Introduction to Thermostatistics”, John Wiley & Sons (1985).
- [Cam14] A. del Campo, J. Goold, and M. Paternostro, “More bang for your buck: Super-adiabatic quantum engines”, *Scientific Reports* **4**, 6208 (2014).
- [Car72] S. Carnot, “Réflexions sur la puissance motrice du feu et sur les machines propres à développer cette puissance”, *Annales scientifiques de l’École normale supérieure* **1**, 393 (1872).
- [Che10] X. Chen, A. Ruschhaupt, S. Schmidt, A. del Campo, D. Guéry-Odelin, and J. G. Muga, “Fast Optimal Frictionless Atom Cooling in Harmonic Traps: Shortcut to Adiabaticity”, *Physical Review Letters* **104**, 063002 (2010).

- [Che11] X. Chen, E. Torrontegui, D. Stefanatos, J.-S. Li, and J. G. Muga, “Optimal trajectories for efficient atomic transport without final excitation”, *Physical Review A* **84**, 043415 (2011).
- [Cur75] F. L. Curzon and B. Ahlborn, “Efficiency of a Carnot engine at maximum power output”, *American Journal of Physics* **43**, 22 (1975).
- [Dan19a] R. Dann and R. Kosloff, “Quantum Signatures in the Quantum Carnot Cycle”, eprint: arXiv:1906.06946 (2019).
- [Dan19b] R. Dann, A. Tobalina, and R. Kosloff, “Shortcut to Equilibration of an Open Quantum System”, *Phys. Rev. Lett.* **122**, 250402 (2019).
- [Den13] J. Deng, Q.-h. Wang, Z. Liu, P. Hänggi, J. Gong, J. Deng, Q.-h. Wang, Z. Liu, P. Hänggi, and J. Gong, “Boosting work characteristics and overall heat-engine performance via shortcuts to adiabaticity: Quantum and classical systems”, *Physical Review E* **88**, 062122 (2013).
- [Die93] R. Diesel, “Theorie und Konstruktion eines rationellen Wärmemotors”, Springer Berlin Heidelberg (1893).
- [Erm08] V. Ermakov, “Second-order differential equations: Conditions of complete integrability”, *Applicable Analysis and Discrete Mathematics* **2**, 123 (2008).
- [Esp10a] M. Esposito, R. Kawai, K. Lindenberg, and C. V. den Broeck, “Efficiency at Maximum Power of Low-Dissipation Carnot Engines”, *Physical Review Letters* **105**, 150603 (2010).
- [Esp10b] M. Esposito, R. Kawai, K. Lindenberg, and C. V. den Broeck, “Quantum-dot Carnot engine at maximum power”, *Physical Review E* **81**, 041106 (2010).
- [Gev92a] E. Geva and R. Kosloff, “A quantum-mechanical heat engine operating in finite time. A model consisting of spin-1/2 systems as the working fluid”, *The Journal of Chemical Physics* **96**, 3054 (1992).
- [Gev92b] E. Geva and R. Kosloff, “On the classical limit of quantum thermodynamics in finite time”, *The Journal of Chemical Physics* **97**, 4398 (1992).
- [Glo15] T. F. Gloger, P. Kaufmann, D. Kaufmann, M. T. Baig, T. Collath, M. Johanning, and C. Wunderlich, “Ion-trajectory analysis for micromotion minimization and the measurement of small forces”, *Physical Review A* **92**, 043421 (2015).
- [Goe15] M. H. Goerz, “Optimizing Robust Quantum Gates in Open Quantum Systems”, Universität Kassel (2015).
- [Hai03] E. Hairer, C. Lubich, and G. Wanner, “Geometric numerical integration illustrated by the Störmer–Verlet method”, *Acta Numerica* **12**, 399 (2003).
- [Het15] M. Hettrich, T. Ruster, H. Kaufmann, C. Roos, C. Schmiegelow, F. Schmidt-Kaler, and U. Poschinger, “Measurement of Dipole Matrix Elements with a Single Trapped Ion”, *Physical Review Letters* **115**, 143003 (2015).

- [Jon97] R. M. Jones, D. Gerlich, and S. L. Anderson, “Simple radio-frequency power source for ion guides and ion traps”, *Review of Scientific Instruments* **68**, 3357 (1997).
- [Kau17] H. Kaufmann, T. Ruster, C. Schmiegelow, M. Luda, V. Kaushal, J. Schulz, D. von Lindenfels, F. Schmidt-Kaler, and U. Poschinger, “Scalable Creation of Long-Lived Multipartite Entanglement”, *Physical Review Letters* **119**, 150503 (2017).
- [Kha05] N. Khaneja, T. Reiss, C. Kehlet, T. Schulte-Herbrüggen, and S. J. Glaser, “Optimal control of coupled spin dynamics: design of NMR pulse sequences by gradient ascent algorithms”, *Journal of Magnetic Resonance* **172**, 296 (2005).
- [Kon03] B. Kongtragool and S. Wongwises, “A review of solar-powered Stirling engines and low temperature differential Stirling engines”, *Renewable and Sustainable Energy Reviews* **7**, 131 (2003).
- [Kos14] R. Kosloff and A. Levy, “Quantum Heat Engines and Refrigerators: Continuous Devices”, *Annual Review of Physical Chemistry* **65**, 365 (2014).
- [Kos17] R. Kosloff and Y. Rezek, “The Quantum Harmonic Otto Cycle”, *Entropy* **19**, 136 (2017).
- [Kos84] R. Kosloff, “A quantum mechanical open system as a model of a heat engine”, *The Journal of Chemical Physics* **80**, 1625 (1984).
- [Kre05] A. Kreuter, C. Becher, G. P. T. Lancaster, A. B. Mundt, C. Russo, H. Häffner, C. Roos, W. Hänsel, F. Schmidt-Kaler, R. Blatt, and M. S. Safronova, “Experimental and theoretical study of the $3d^2D$ -level lifetimes of $^{40}\text{Ca}^+$ ”, *Physical Review A* **71**, 032504 (2005).
- [Lei03] D. Leibfried, R. Blatt, C. Monroe, and D. Wineland, “Quantum dynamics of single trapped ions”, *Reviews of Modern Physics* **75**, 281 (2003).
- [Lem13] A. Lemmer, A. Bermudez, and M. B. Plenio, “Driven geometric phase gates with trapped ions”, *New Journal of Physics* **15**, 083001 (2013).
- [Lev17] A. Levy, E. Torrontegui, and R. Kosloff, “Action-noise-assisted quantum control”, *Physical Review A* **96**, 033417 (2017).
- [Lev18] A. Levy, A. Kiely, J. G. Muga, R. Kosloff, and E. Torrontegui, “Noise resistant quantum control using dynamical invariants”, *New Journal of Physics* **20**, 025006 (2018).
- [Lew69] H. R. Lewis and W. B. Riesenfeld, “An Exact Quantum Theory of the Time-Dependent Harmonic Oscillator and of a Charged Particle in a Time-Dependent Electromagnetic Field”, *Journal of Mathematical Physics* **10**, 1458 (1969).
- [Ma17] Y.-H. Ma, S.-H. Su, and C.-P. Sun, “Quantum thermodynamic cycle with quantum phase transition”, *Physical Review E* **96**, 022143 (2017).
- [Ma18] Y.-H. Ma, D. Xu, H. Dong, and C.-P. Sun, “Optimal operating protocol to achieve efficiency at maximum power of heat engines”, *Physical Review E* **98**, 022133 (2018).

- [Møl99] K. Mølmer and A. Sørensen, “Multiparticle Entanglement of Hot Trapped Ions”, *Physical Review Letters* **82**, 1835 (1999).
- [Nie09] M. A. Nielsen and I. L. Chuang, “Quantum Computation and Quantum Information”, 10th ed., 10th ed., Cambridge University Press (2009).
- [Nil88] H. Nilsson, “Submarine Power Systems Using the V4-275R Stirling Engine”, *Proceedings of the Institution of Mechanical Engineers, Part A: Power and Process Engineering* **202**, 257 (1988).
- [Nov58] I. Novikov, “The efficiency of atomic power stations (a review)”, *Journal of Nuclear Energy (1954)* **7**, 125–128 (1958).
- [Pal16] M. Palmero, S. Wang, D. Guéry-Odelin, J.-S. Li, and J. G. Muga, “Shortcuts to adiabaticity for an ion in a rotating radially-tight trap”, *New Journal of Physics* **18**, 043014 (2016).
- [Ram13] M. Ramm, T. Pruttivarasin, M. Kokish, I. Talukdar, and H. Häffner, “Precision Measurement Method for Branching Fractions of Excited $P_{1/2}$ States Applied to $^{40}\text{Ca}^+$ ”, *Physical Review Letters* **111**, 023004 (2013).
- [Rei15] D. M. Reich, “Efficient Characterisation and Optimal Control of Open Quantum Systems - Mathematical Foundations and Physical Applications”, Universität Kassel (2015).
- [Roß14] J. Roßnagel, O. Abah, F. Schmidt-Kaler, K. Singer, and E. Lutz, “Nanoscale Heat Engine Beyond the Carnot Limit”, *Physical Review Letters* **112**, 030602 (2014).
- [Roß15] J. Roßnagel, K. N. Tolazzi, F. Schmidt-Kaler, and K. Singer, “Fast thermometry for trapped ions using dark resonances”, *New Journal of Physics* **17**, 045004 (2015).
- [Roß16a] J. Roßnagel, “A Single-Atom Heat Engine”, Dissertation, Johannes Gutenberg-Universität Mainz (2016).
- [Roß16b] J. Roßnagel, S. T. Dawkins, K. N. Tolazzi, O. Abah, E. Lutz, F. Schmidt-Kaler, and K. Singer, “A single-atom heat engine”, *Science* **352**, 325 (2016).
- [Sak17] J. J. Sakurai and J. Napolitano, “Modern Quantum Mechanics”, 2nd ed., 2nd ed., Cambridge University Press (2017).
- [Sas62] F. Sass, “Otto erfindet den Viertaktmotor (1876)”, Springer Berlin Heidelberg (1962),
- [Sch03] F. Schmidt-Kaler, H. Häffner, M. Riebe, S. Gulde, G. P. T. Lancaster, T. Deuschle, C. Becher, C. F. Roos, J. Eschner, and R. Blatt, “Realization of the Cirac–Zoller controlled-NOT quantum gate”, *Nature* **422**, 408 (2003).
- [Sin10] K. Singer, U. Poschinger, M. Murphy, P. Ivanov, F. Ziesel, T. Calarco, and F. Schmidt-Kaler, “Colloquium: Trapped ions as quantum bits: Essential numerical tools”, *Reviews of Modern Physics* **82**, 2609 (2010).
- [Siv12] J. D. Siverns, L. R. Simkins, S. Weidt, and W. K. Hensinger, “On the application of radio frequency voltages to ion traps via helical resonators”, *Applied Physics B* **107**, 921 (2012).

- [Ste10] D. Stefanatos, J. Ruths, and J.-S. Li, “Frictionless atom cooling in harmonic traps: A time-optimal approach”, *Physical Review A* **82**, 063422 (2010).
- [Tan09] T. Tang and C. Burkhardt, “Hybrid MOSFET/driver for ultra-fast switching”, *IEEE Transactions on Dielectrics and Electrical Insulation* **16**, 967 (2009).
- [Tor12] E. Torrontegui, S. Martínez-Garaot, A. Ruschhaupt, and J. G. Muga, “Shortcuts to adiabaticity: Fast-forward approach”, *Physical Review A* **86**, 013601 (2012).
- [Tor13a] E. Torrontegui and R. Kosloff, “Quest for absolute zero in the presence of external noise”, *Physical Review E* **88**, 032103 (2013).
- [Tor13b] E. Torrontegui, S. Ibáñez, S. Martínez-Garaot, M. Modugno, A. del Campo, D. Guéry-Odelin, A. Ruschhaupt, X. Chen, and J. G. Muga, “Chapter 2 - Shortcuts to Adiabaticity”, *Advances in Atomic, Molecular, and Optical Physics*, ed. by E. Arimondo, P. R. Berman, and C. C. Lin, vol. 62, *Advances In Atomic, Molecular, and Optical Physics*, Academic Press (2013), 117–169.
- [Tor17] E. Torrontegui, I. Lizuain, S. González-Resines, A. Tobalina, A. Ruschhaupt, R. Kosloff, and J. G. Muga, “Energy consumption for shortcuts to adiabaticity”, *Physical Review A* **96**, 022133 (2017).
- [Tor18] E. Torrontegui, S. T. Dawkins, M. Göb, and K. Singer, “Transient non-confining potentials for speeding up a single ion heat pump”, *New Journal of Physics* **20**, 105001 (2018).
- [Tur00] Q. A. Turchette, C. J. Myatt, B. E. King, C. A. Sackett, D. Kielpinski, W. M. Itano, C. Monroe, and D. J. Wineland, “Decoherence and decay of motional quantum states of a trapped atom coupled to engineered reservoirs”, *Physical Review A* **62**, 053807 (2000).
- [Wee12] C. Weedbrook, S. Pirandola, R. García-Patrón, N. J. Cerf, T. C. Ralph, J. H. Shapiro, and S. Lloyd, “Gaussian quantum information”, *Reviews of Modern Physics* **84**, 621 (2012).
- [Wu98] F. Wu, L. Chen, F. Sun, C. Wu, and Y. Zhu, “Performance and optimization criteria for forward and reverse quantum Stirling cycles”, *Energy Conversion and Management* **39**, 733 (1998).
- [Yin17] Y. Yin, L. Chen, and F. Wu, “Optimal power and efficiency of quantum Stirling heat engines”, *The European Physical Journal Plus* **132**, 45 (2017).
- [Yin18] Y. Yin, L. Chen, and F. Wu, “Performance of quantum Stirling heat engine with numerous copies of extreme relativistic particles confined in 1D potential well”, *Physica A: Statistical Mechanics and its Applications* **503**, 58 (2018).

Acknowledgments

Without my colleagues and friends, who I value and hold dear, this work would not be possible. Therefore, I want to thank those amazing people, I met along the way.

First of all, I like to thank Prof. Dr. Kilian Singer for many inspiring discussions. I am utterly grateful for the trust he put in me. Not only to work on the paper we published, but also to do laboratory preparations with many freedoms. Dr. Sam Dawkins instructed me as well, which I greatly appreciate.

Furthermore, I like to thank Dr. Erik Torrontegui for many interesting discussions and for giving me a good insight into the methods of STA. Without his help, I might not have comprehended the underlying principles.

I thank Daqing for supervising me and leading the project carefully. Since his arrival, strong advancement in the Laboratory has occurred.

I am also grateful for meeting Dr. Dawid Crivelli, who not only taught me the basics of quantum optics but also started my interest in the project. Unfortunately, he could not supervise my thesis.

I also want to thank the current and former members of the light-matter-interaction group of Prof. Dr. Kilian Singer at the University of Kassel for many insightful discussions and helpful remarks. These members are Josselin Bernardoff, Bo Deng, Miriam Mendoza Delgado, Dr. Peter Zahariev, Stefan Aull, Florian Elsen, Ricky-Joe Plate, Simon Schott, Jan Thieme, Nick Vogeley, Jan Jakob, Thorben Benno Muehleder, and Michael Schulz .

Furthermore, I like to thank the administrative staff Andreas Arend, Cornelia Moritz, and Gabriele Schoenewolf-Kuppstadt as well, for assisting me in handling various requests and forms.

I like to thank Dr. Daniel Reich and Daniel Basilewitsch, who showed an incredible amount of patience explaining theoretical and numerical principles to me. Furthermore, I am grateful for the very insightful discussions and fascinating considerations with Yu-Han Ma, Dr. Amikam Levy, and Prof. Dr. Ronnie Kosloff.

I greatly appreciate the time I spent studying with my fellow students, where we had much fun discussing sometimes strange but interesting topics. I like to thank especially Stephen Eggebrecht, Jonas Kalveram, Pascal Plettenberg, and Varazdat Grigorian, just to name a few.

Finally, I want to express my deepest gratitude for the support my family gave me. Especially I want to thank my mother and my brother for giving me not just emotional but also financial support.